Biomarker stratigraphy in the Athel Trough of the South Oman Salt Basin at the Ediacaran#Cambrian Boundary

Biomarker stratigraphy in the Athel Trough of the South Oman Salt Basin at the Ediacaran-Cambrian Boundary

Anaïs Roussel[1, 2], Xingqian Cui[1,3*], Roger E. Summons[1*]

[1]Department of Earth, Atmospheric, and Planetary Sciences, Massachusetts Institute of Technology, Cambridge, MA, USA

[2]Now at Department of Biology, Georgetown University, Washington, DC, USA

[3]School of Oceanography, Shanghai Jiao Tong University, 1954 Huashan Road, Shanghai 200030, China

[*]Corresponding Authors: rsummons@mit.edu and xcui@mit.edu

Highlights:

1) High resolution biomarker chemostratigraphy reveals microbial community and redox variability through the Ediacaran-Cambrian transition at the Athel Trough of the South Oman Salt Basin
2) Low concentrations of aromatic carotenoids from GSB and PSB suggest weak or episodic photic zone euxinia
3) Unusual patterns of aromatic carotenoids, distinct from those most commonly seen in most Phanerozoic sediments and oils, are consistent with contributions from cyanobacteria

Abstract

The South Oman Salt Basin (SOSB) has been studied extensively for knowledge concerning the habitat of the enigmatic Ediacaran-Cambrian oils that are produced from that region. Geological, geochemical, geophysical and geochronological investigations have all contributed to improved understanding of the range of late Neoproterozoic depositional environments recorded there. Of particular interest has been the deep Athel depocenter within the SOSB that features a silica rich interval known as the Al Shomou Member or Athel Silicilyte and the co-eval A4 carbonate evaporite sequence that straddles the Ediacaran-Cambrian boundary. The deep basin has been suggested to be anoxic and euxinic based on studies of sulfur isotopes, trace metal distributions and other proxies. Organic geochemistry has provided some clues concerning aspects of the depositional environments and microbial communities prevailing during this interval. However, ambiguities remain including a paucity of convincing molecular evidence for euxinia in the photic zone of the basin. Here, we present a comprehensive study of biomarker hydrocarbons, including steroids, triterpenoids and carotenoids. Among the compounds detected is a distinctive array of aromatic carotenoids. Relatively low abundances of monoaromatic carotenoids, such as chlorobactane, okenane and β-isorenieratane, suggest the possibility of transient photic zone euxinia with a shallow chemocline or, perhaps, exogenous inputs from microbial mats. However, it is the dominance of renieratane and renierapurpurane over isorenieratane in diaromatic carotenoids and their association with abundant C_{38} and C_{39} carotenoids that identifies cyanobacteria as major contributors to the inventory of carotenoids. Our results, based on multiple lines of molecular evidence and statistical analysis, also suggest that the Athel Silicilyte was biogeochemically distinct from the other units of the Ara Group. Overall, our study has important implications for understanding other late Neoproterozoic depositional environments.

Introduction

Over recent decades, the South Oman Salt Basin (SOSB) has attracted attention owing to the presence of commercial oil deposits derived from Neoproterozoic-Cambrian sedimentary sequences. The very unusual biomarker characteristics of the early SOSB oil discoveries enabled their attribution to units within the Huqf Supergroup (Grantham et al., 1988a; Terken et al., 2001), a thick sequence of rocks that covers most of the ~635 to ~541 Ma Ediacaran Period. A sequence within the Huqf Supergroup, the Ara Group is of special biogeochemical and paleontological interest as these sediments span the Ediacaran-Cambrian boundary. Where represented by a shallow carbonate platform, the Ara sequence is comprised of up to

seven carbonate-evaporite cycles denoted A0 to A6 (Grotzinger and Al-Rawahi, 2014). Rifting at ~543 Ma during the deposition of the fourth of these cycles, denoted as the A4, resulted in a package of sediments including more clastic material deposited in the deeper Athel sub-basin. It is composed of the Al Shomou Member of the Athel Formation or Athel Silicilyte (Al Rajaibi et al., 2015; Amthor et al., 2015) and is bracketed by the U Shale Member below and the Thuleilat Shale Member above. All three sedimentary units were deposited under anoxic conditions. The sequences and composition of evaporites show that the waters of the SOSB were rich in sulfate while the prevalence of pyrite combined with trace metal and biomarker data suggest that euxinic conditions prevailed in the water column during deposition of the deep basinal facies (Grantham et al., 1988a; Grosjean et al., 2009; Schroder and Grotzinger, 2007; Stolper et al., 2017). However, none of these previous studies reported convincing evidence for photic zone euxinia (PZE) during deposition of the Athel Formation.

Photic zone euxinia is the phenomenon where sulfidic waters protrude into the euphotic zone thereby permitting anoxygenic photosynthesis by the green sulfur bacteria (GSB) and purple sulfur bacteria (PSB) and giving rise to an array of distinctive aromatic carotenoid and chlorophyll pigments. The aromatic carotenoids, which are widely observed in sediments deposited over the Phanerozoic Eon, and especially during oceanic anoxic events (French et al., 2015; Whiteside and Grice, 2016), are rarely reported in Pre-Cambrian strata. Nevertheless, the oldest aromatic carotenoids were discovered in the a lagoonal facies of the Barney Creek Formation at 1.6 Ga in the Paleoproterozoic Era (Brocks et al., 2005). Additionally, a few studies have reported aromatic carotenoids in the Neoproterozoic Era (Bhattacharya et al., 2017; French et al., 2015). Recently, two aromatic carotenoids (i.e., chlorobactane, okenane) were detected for the first time in the SOSB (French et al., 2015), thereby prompting further detailed investigation on the evidence for PZE in this depositional system.

A variety of other hydrocarbon biomarkers have been commonly applied in the study of microbial communities in modern and ancient settings (Peters et al., 2005). This is based on the idea that a certain subset of compounds is synthesized by a limited number of specific organisms and under particular environmental conditions (Table 1). Most commonly, steranes and hopanes are the fossilized remains of sterols and hopanoids synthesized by eukaryotes and bacteria, respectively. Another common sedimentary biomarker is gammacerane,

regarded as a diagenetic product of tetrahymanol derived from protists living at redox boundaries in stratified water columns (Harvey and Mcmanus, 1991). In this study, we measured patterns of biomarkers aiming to shed further light on the dynamic evolution of environments across the Ediacaran-Cambrian boundary in deep basinal sediments of the SOSB and on the depositional conditions and microbial processes taking place during deposition of the enigmatic Athel Silicilyte.

The Athel Silicilyte, which was deposited at the same time as the A4C unit on the carbonate platform, provides an archive to investigate the characteristics of deep-water environments in relation to shallow water analogues. Distinct from the carbonate platform, which can be biased by benthic microbial mats or terrigenous inputs, the Silicilyte deposits in the Athel deep basin record the signal best representative of the microbial communities in the water column and is ideal for testifying the presence of anoxygenic phototrophs at the Ediacaran-Cambrian transition. While this study only focuses on one well (Athel-1), our regional data extrapolation is based on comparison with samples from shallow carbonate platforms, previously published oils and rocks (Grosjean et al., 2009), and another section further west (Marmul Northwest-7; Figure 1) that were studied in earlier research (Stolper et al., 2017).

2. Regional Geological Setting

The stratigraphic sequence of South Oman is characterized by an early Neoproterozoic non-sedimentary basement overlain unconformably by the Huqf Supergroup dated as Neoproterozoic to earliest Cambrian. The Huqf Supergroup is distinguished from the overlying Haima Supergroup of middle Cambrian to Silurian age by a regional unconformity. It is now recognized that the Huqf Supergroup holds valuable information on petroleum formation, basin development, climate conditions and evolution of the biosphere over the Neoproterozoic-early Cambrian (Allen, 2007; Bowring et al., 2007).

The Huqf Supergroup is subdivided into three distinct sedimentary units. In an ascending order, they are the Abu Mahara Group, the Nafun Group, and the Ara Group (Figure 1). The lowermost Abu Mahara Group, time equivalent to the Sturtian and Marinoan Snowball Earth events, features glacial clastics capped by a carbonate layer that signals post-glacial transgression. The Nafun group above the cap carbonate consists of two siliciclastic to carbonate cycles (Aitken, 1966). The Nafun Group witnessed the broadening of the subsiding basin, possibly related to the post-rift thermal contraction of the lithosphere (Kapellos et al.,

1992) or the subduction of oceanic lithosphere into the mantle (Grotzinger et al., 2002; Gurnis, 1988, 1992). The Nafun Group-Ara Group boundary marks the uplift of basin basement blocks and the subsequent segmentation of the broader Nafun basin into three fault-bounded sub-basins, namely as the South Oman Salt Basin (SOSB), the Ghaba Salt Basin, and the Fahud Salt Basin.

The ensuing Ara Group records further segmentation of each sub-basin with polarized sedimentation, a shift toward arid climatic conditions and accumulation of evaporative salt sequences. Within the SOSB, further segmentation subdivided the SOSB into three domains, namely as the Northern Carbonate Domain, the Athel deep sub-sub-basin (a.k.a. Athel Trough), and the Southern Carbonate Domain (Figure 1), related to uneven basement subsidence rates (Grotzinger et al., 2002). The stratigraphy of the two carbonate domains comprises up to seven carbonate-evaporite cycles designated as A0 to A6 (Grotzinger and Al-Rawahi, 2014). Each cycle starts with deposition of evaporites at lowstand and is topped by carbonates formed during highstand consequent from a renewed infusion of seawater. Such water depth and salinity cycles are explained by a tectonic-eustatic model with periodic connections to the open ocean (Allen, 2007; Amthor et al., 2002). The stratigraphy of the Ara Group in the Athel trough displays the majority of carbonate-evaporite cycles present on the carbonate platforms and, additionally, includes a thick and unique unit rich in clays and silica (Figure 1). This layer is equivalent in time to the A4 carbonate deposition (A4C) and is bracketed by the A4 and A5 evaporite cycles (A4E and A5E). Since the lithologies of this layer are heterogeneous, it is further subdivided into the U Shale Member, the Al Shomou Silicilyte Member, and the Thuleilat Shale Member (Forbes et al., 2010), representing a transgression-regression sequence with sea level peaked during the Al Shomou Silicilyte Member. Microstructural studies have revealed micron scaled lamination in the Silicilyte matrix intercalated with organic matter-rich and finely crystalline quartz-rich layers. Other minerals of diagenetic origin include pyrite, apatite, dolomite, magnesite and barite (Amthor et al., 2015). All three units are estimated to be deposited under a minimum water depth of ~200m (Amthor et al., 1998). This implies that the Athel deep basin continued subsiding while the carbonate platforms remained uplifted during A4 time. Although the mechanisms for such disparate eustatic rebound are not well understood, it is clear that the depositional environment of the SOSB was not uniform throughout the Ara Group.

Pertinent to the molecular analyses discussed below, carbon and sulfur isotopic analyses of SOSB sediments speak to the ocean becoming increasingly oxygenated during deposition of the Huqf Supergroup (Canfield et al., 2010; Fike et al., 2006; Leavitt et al., 2013; Sim et al., 2011). Sulfur isotopic data, in particular, show a progressive increase in $\Delta\delta^{34}S$ throughout deposition of the Nafun Group to values sometimes in excess of 46‰ by the end of Buah time. This value approaches the maximal fractionation expressed by bacterial sulfate reduction, indicates the presence of a significant marine sulfate inventory and implies a substantial pool of H_2S persistent in the SOSB (Fike and Grotzinger, 2008, 2010). Above the Nafun Group, paired sulfate–pyrite $\delta^{34}S$ data for sediments of the Ara evaporite cycles deposited just prior to, and through the Ediacaran-Cambrian Boundary, show anomalous enrichments in both $\delta^{34}S_{sulfate}$ and $\delta^{34}S_{pyrite}$ interpreted as an increase in pyrite burial potentially driven by a substantial iron supply, supporting possible ferruginous ocean conditions at the Ediacaran-Cambrian transition (Fike & Grotzinger, 2010). Thus, the sulfur isotopic data for the SOSB indicate a very active biogeochemical sulfur cycle with substantial pyrite deposition but also the possibility of supporting the activities of anoxygenic phototrophs that utilize sulfide as an electron donor for photosynthetic carbon fixation.

2. Materials and Methods

2.1. Samples and Preparation

We focus primarily on the A4-equivalent units of the Athel-1 well drilled in the deep basin near the Eastern Flank Platform in order to better constrain depositional environment of the Silicilyte and bounding shale formations in the deep basin (Figure 1). The Silicilyte Member here is ~300m thick, finely laminated, rich in organic carbon and composed of 80-90% microcrystalline quartz. In this well it is bounded by the Thuleilat Shale member above (~1125m) and the U Shale Member below (~1425m). It was proposed that the water depth of the deep basin increased to the maximum of ~100200m (Schröder et al., 2003) or >200m (Amthor et al., 1998; Amthor et al., 2002) during deposition of the Silicilyte. The base of the Silicilyte was deposited during the early Cambrian (541±0.13Ma), when the major diversification of the metazoan phyla took place (Erwin, 2015).

In this study, we examined a total of twenty-one cleaned cuttings samples from the Athel-1 well covering a depth from 1051m to 1602m, with three samples from the Thuleilat Shale, eleven from the Silicilyte and seven from the U Shale. For comparison, we also included eight additional samples from the Shuram and Buah formations from Athel-1 well and the A4

carbonate from Birba-3 well (Figure 1). Specifically, samples from the Silicilyte were selected to ensure thorough coverage of the unit. Furthermore, the Silicilyte Member is divided into upper and lower units, based on gamma ray data. Cuttings samples (1–2 g) were placed in a puck mill and powdered in a shatterbox. The mill was cleaned sequentially with fired sand, DI water, methanol and DCM between samples, to avoid cross-contamination.

2.2. Bulk OC and $\delta^{13}C$ Measurements

About 0.3g of each ground sample was decarbonated using 1N HCl. The supernatant was decanted after centrifuging. The precipitated particles were further rinsed several times with Millipore water to remove residual acid. The decarbonated residuals were dried at 60°C, followed by grinding by hand with a mortar and pestle. The samples were weighted into tin capsules and introduced to an autosampler. Total organic carbon, carbon isotopes and nitrogen isotopes were measured on an elemental analyzer (EA) coupled to an isotope ratio mass spectrometer (IRMS). Instrumental precision based on duplicate measurements of USGS 40 standard was 0.11‰ for $\delta^{13}C$ values.

2.3. Biomarker Analysis

About 0.7g of each ground sample was extracted with DCM:MeOH (9:1), using a Dionex Accelerator Solvent Extractor 350 (ASE), operated at 100°C. Total solvent extracts were re-dissolved in ~1ml pentane to induce asphaltene precipitation, which was removed after centrifugation. Elemental sulfur was removed by the addition of activated copper shot which was then removed by centrifugation. The resultant extracts were dried to <100ul and fractionated on a silica gel column. Hexane : dichloromethane (4:1; v:v) and dichloromethane : methanol (4:1;v:v) were used to elute the non-polar and polar fractions, sequentially.

The non-polar fraction was analyzed on an Agilent gas chromatograph (GC, 7890B) coupled to an Agilent triple quadrupole MS (QQQ, 7010A) operated in multiple reaction monitoring (MRM) mode (Table S1). A multi-mode injector with an initial injection temperature of 45°C was ramped at a rate of 720°/min to 340°C. A DB-5MS column (60m×250µm×0.25µm) was installed with the GC oven temperature held isothermally at 40° for 2 mins, ramped to 320°C at a rate of 4°/min, and then held at this temperature for 22 mins. The transfer line and source temperatures were set at 300° and 250°, respectively. The electron energy was set at 50eV to ensure a stronger signal for the precursor-product transitions. All biomarker data were processed using MassHunter QQQ software. Each compound was identified and integrated

under MRM mode within a narrow retention time window (0.5min). For quality control, four samples were randomly selected for duplicate measurements and error bars indicated in figures represent standard deviation.

2.4. Statistical Analysis

Two-tailed unequal variance *t*-tests were performed to determine significant differences between independent groups of variables, while one-tailed unequal variance *t*-tests were applied when comparing for higher or lower values (e.g., Thuleilat vs Silicilyte). A *p* value of < 0.05 was considered as significant, while $0.05 < p < 0.1$ was considered as weakly significant, however, caution was exercised when a group contains limited number of samples. Principal components analysis (PCA) was performed to discriminate controlling variables linked with bulk and biomarker patterns. Cluster Analysis was performed to categorize individual samples into groups based on proxy similarities. The Thuleilat Shale, upper Silicilyte Member, lower Silicilyte Member and U Shale were treated separately in the comparison.

3. Results and Discussion

3.1. Maturity and the potential for oil migration

The thermal maturity of these three units (the U Shale Member, the Al Shomou Silicilyte Member, and the Thuleilat Shale Member) from Athel-1 well were assessed earlier using composite cuttings samples, where Rock-Eval T_{max} values range from 419 to 430 °C (Grosjean et al., 2009). The molecularly-based thermal maturity parameters presented here confirm a relatively mild thermal history.

The C_{27} hopane Tm, with its 17β(H) configuration 17β(H)-22,29,30-trisnorhopane, is thermodynamically less stable than the neohopane Ts 18α(H)-22,29,30-trisnorneohopane, hence, the Ts/(Ts+Tm) ratio is widely observed to gradually increase with increasing burial depth and maturation process (Peters et al., 2005). The ratios of Ts/(Ts+Tm) varied between 0.18 and 0.29 (Table 2; Figure S1), lower and narrower compared to those reported previously for the Marmul Northwest-7 well (Stolper et al., 2017). Other maturity indices further constrain the samples being placed in the early oil generation window. For example, the C_{31}H S(S+R) ratios are based on the thermally-driven isomerization at C-22 position of hopane side-chain during maturation. The C_{31}H S/(S+R) ratios from this study are broadly constant and fell in a range between 0.51 and 0.57 (Figures S1, S3), placing samples in the

early (0.50 – 0.54) and the earliest stage of main oil generation (0.57 – 0.64) windows (Seifert and Moldowan, 1980). Additionally, the comparable isomer ratios for the steranes, exemplified by the C_{29}S ααα S/(S+R), which is based on the isomerization of C_{29} 5α,14α,17α steranes at C-20 (R, S), ranged between 0.46 and 0.52 (Table 2; Figures S2, S3), lower than the maximum equilibrium value of 0.52-0.55 (Seifert and Moldowan, 1986). So, together, these parameters suggest that the entire section is in the earliest stages of oil generation.

In contrast, some parameters display distinct ranges that do not match with the earliest oil generation window or expected maturation trend down section (e.g., Ts/(Ts+Tm)), suggesting that other factors, including organic facies and sediment lithologies (Moldowan et al., 1986; Seifert and Moldowan, 1986), are playing a prominent role in modulating thermal-maturity-related proxies. For example, the C_{30}H βα/(αβ+βα) ratio, otherwise known as moretane/(moretane+hopane) ratio, involves conversion of 17β,21α-hopanes (moretanes) to 17α,21β-hopanes at elevated temperatures, resulting in an equilibrium mixture of βα-hopanes over αβ-hopanes at a ratio ~ 0.05 (Peters et al., 2005). Therefore, samples pre-equilibrium are expected to have C_{30}H βα/(αβ+βα) ratios >0.05. In the present study, C_{30}H βα/(αβ+βα) ratios exhibited a narrow range between 0.03 and 0.04, even lower than the suggested equilibrium ratio of 0.05 (Figure S3). Additionally, remarkably low proportions of diasteranes (0.02 – 0.07), defined as C_{29} dia/(dia+reg), are observed in the Silicilyte Member as compared to the bounding clastic units (Figure S3) and affirm the idea that lithological features, and especially low clay contents (French et al., 2012; van Kaam-Peters et al., 1998), as well as redox conditions experienced during diagenesis, influence processes involved in the epimerization and rearrangement reactions that underpin these maturity proxies (Peters et al., 2005).

Overall, stratigraphic variability in thermal maturity proxies is observed down section. Notably, the much lower C_{31}H S(S+R) values (0.51-0.54) are observed in the Thuleilat Shale than the underlying units (0.55-0.57; $p < 0.05$), while the lowest Ts/(Ts+Tm) values are found in the U Shale (Figures S1, S3). In addition to the lowest C_{29} dia/(dia+reg) sterane ratios in the Silicilyte Member, C_{29}S ααα S/(S+R) ratios decrease down section, opposite to the normal expectation. Stratigraphically, stratigraphic heterogeneity in thermal maturity indices and biomarker distributions (discussed below), in concert with the presence of impermeable evaporite layers (A4 and A5) strongly argues against oil migration and post-depositional overprinting. Furthermore, mild Rock-Eval T_{max} values (419 – 430 °C) indicate immature source rocks in the Athel-1 well (Grosjean et al., 2009). Overall, it is very likely that oils

found in the Silicilyte Member were self-sources and experienced minimal migration, validating paleoenvironmental reconstruction based on organic proxies.

3.2. Microbial community changes during basin development

Organic carbon contents ranged between 1.53% and 8.89%. Other than some higher values found in the Thuleilat Shale and U Shale, no obvious trend was observed down-core, which precludes the dependency of biomarker trends on organic carbon contents. Carbon isotopic values ($\delta^{13}C$) for bulk organic carbon spanned a large range from -34.2‰ to -40.6‰. Such low $\delta^{13}C$ values are typical for Huqf sediments and oils (Grantham et al., 1988b; Grosjean et al., 2009), nevertheless, significant differences in $\delta^{13}C$ values were not observed between any two groups of samples (Table 2). Consistent with previous studies, biomarker parameters display significant variations of microbial communities (Grosjean et al., 2009; Love et al., 2009; Stolper et al., 2017). Hopanes and steranes are the two major groups of compounds typically attributed to bacteria and eukaryotes, respectively (Damsté and Koopmans, 1997; Peters et al., 2005), and therefore the sterane/hopane ratio is indicative of relative community density of eukaryotes versus bacteria. At the early stage of U Shale deposition, algae (i.e. eukaryotes) were a significant component of the microbiota as indicated by sterane/hopane ratios in excess of 1 (Figure 2). The deposition of the U Shale records a period of transgression, coupled with fresh intrusions of oxygenated seawater and tectonic subsidence in the deep basin (Grotzinger and Al-Rawahi, 2014). Sterane/hopane ratios >1 are typical of crude oils and source rocks deposited in open marine environments (Moldowan et al., 1985; Schiefelbein et al., 1999). However, this contrasts with sterane/hopane ratios as low as 0.01 in contemporaneous oligotrophic settings deposited in Baltica (Pehr et al., 2018), suggesting that other factors including the availability of nutrients may also have been important in determining the relative proportion of eukaryotes and bacteria in marine environments at this time.

Consistent with elevated sterane/hopane ratios during transgression, the highest levels of C_{30} steranes, including 24-*n*-propylcholestane (C_{30}-npc) and 24-*i*-propylcholestane (C_{30}-ipc), were also observed in the U Shale (2.0 – 3.4%) (Figure 3). The presence of C_{30}-ipc has been attributed to the emergence of demosponges in the Neoproterozoic (Love et al., 2009). Although C_{30}-npc found in Devonian and younger samples has been attributed to the emergence of marine pelagophyte algae since mid-Paleozoic (Moldowan et al., 1984), its occurrence in Neoproterozoic and early Paleozoic strata has been ascribed to other sources,

possibly including foraminifera and sponges (Gold et al., 2016; Grabenstatter et al., 2013). More recently, another rare C_{30} steroid 26-methylstigmastane, and its co-occurrence with C_{30}-ipc and C_{30}-npc in suites of Neoproterozoic samples attribute all three C_{30} steranes to demosponges (Zumberge et al., 2018), however, is a topic of continuing debate (Hallmann et al., 2019; Love et al., 2019; Nettersheim et al., 2019). Consistent with a source from demosponges, 26-methylstigmastane was consistently present, albeit in trace amounts, in all samples analyzed (Figure S2).

The transition from the U Shale to the Silicilyte in the Athel-1 well records a subtle increase in the relative abundance of prokaryotic biomass, as indicated by lower sterane/hopane ratios above the U Shale/Silicilyte boundary (Figure 2) and a clear shift based on cluster analysis and PCA results, possibly driven by nutrient availability (Figure 4). Concurrently, we observed that the percentages of $C_{29}/(C_{26\text{-}30})$ steranes, representing the proportions of green algae relative to all eukaryotes, increase significantly ($p < 0.01$) from the U Shale (41.9 – 60.8%) to the lower Silicilyte Member (58.3 – 66.5%), where the highest percentages of C_{29} steranes were observed (Figure 3). The prevalence of green algae over other types of algae is a common observation in the Neoproterozoic and early Cambrian in the SOSB and elsewhere, which is further corroborated by our study. A recent study proposed that the rise to prominence of green algae in post-Cryogenian times was triggered by enhanced nutrient supplies generated during deglaciation (Brocks et al., 2017). If this is true, it implies that higher green algae contribution in the lower Silicilyte may also be a consequence of nutrient availability, possibly attributed to terrestrial inputs from the surrounding land (e.g., Eastern Flank Platform) due to basin subsidence, instead of fresh seawater intrusion. 2-Methylhopane index (2-MHI) has been applied as an indicator for cyanobacterial nitrogen fixation, since cyanobacteria fix nitrogen from the atmosphere and many taxa synthesize 2-methylhopanes (Table 2). Therefore, high values of 2-MHI together with low $\delta^{15}N$ values (~0‰) are consequently indicative of strong nitrogen fixation. However, we observed relatively lower 2-MHI (7.0 – 10.3%) in the U Shale and lower Silicilyte when compared with the upper Silicilyte and Thuleilat Shale, and the data from the Marmul Northwest-7 well (Stolper et al., 2017). Additionally, our samples show constantly positive $\delta^{15}N$ values, negating strong atmospheric nitrogen fixation (Pehr et al., 2018). Thus, our data do not support a strong preference for microbial nitrogen fixation, but instead indicate nitrate concentrations sufficient to support primary productivity in the oxygenated nutrient rich surface waters across the U Shale/Silicilyte boundary.

Overall, one of the clearest trends that can be observed in the Athel-1 well is the apparent correlation between the proportions of C_{30} steranes (C_{30}-npc + C_{30}-ipc; $C_{30}/C_{26\text{-}30}$) and C_{26} steranes (27-norcholestanes; $C_{26}/(C_{26\text{-}30})$), of which the latter ones are pronounced but have so far unknown sources in Ediacaran samples. Both parameters decrease to minima just above the U Shale/lower Silicilyte transition, and being anti-correlated with the increasing trend of $C_{29}/(C_{26\text{-}30})$ steranes (Figures 3, 7). Further, the ratio of C_{30}-ipc/C_{30}-npc is anti-correlated with $C_{30}/(C_{26\text{-}30})$ steranes, indicating that C_{30}-ipc, C_{30}-npc and the 27-norcholestanes have discrete sources. Lastly, relative abundances of 3β-methyl-24-ethylcholestanes (3β-Me C_{29}/C_{29}) do not follow those of the 24-ethylcholestanes (C_{29} steranes) but display a trend opposite to that of the sterane/hopane ratios (Figure 2). Therefore, the production of 3β-methyl-24-ethylcholestanes appears to be the consequence of a distinct process and not directly controlled by the relative abundance of green algal sources of the C_{29} steranes. This is consistent with these compounds having a specific biological origin, possibly via bacterial modification of algal sterols.

3.3. Redox conditions and corresponding biological indicators

Pristane/phytane ratios were low throughout the sequence and ranged between 0.14 and 0.73, with significantly lower values in the Silicilyte Member (0.16 – 0.39) than the U Shale (0.24 – 0.44; $p < 0.02$) and the Thuleilat Shale (0.43 – 0.73; $p < 0.04$; Table 2). It points to the existence of water column anoxia throughout the succession, with extremely reducing conditions in the Athel Silicilyte, consistent with previous results from the SOSB (Grosjean et al., 2009; Love et al., 2009; Stolper et al., 2017) and contrasting to the observations made in the contemporaneous oligotrophic setting in Baltica studied by Pehr et al. (2018). Under anoxic conditions, nitrate, sulfate, and CO_2 are sequentially consumed as electron acceptors, with progressively less energy generation, respectively (Amend and Shock, 2001). When nitrate is preferentially consumed, nitrogen fixation from the atmosphere is required to sustain photosynthesis in the photic zone. In this study, relatively high 2-MHI values up to 13.7% in the upper Silicilyte and Thuleilat Shale are comparable to cases of oceanic anoxic events (Kuypers et al., 2004), suggestive of some degree of nitrogen fixation by cyanobacteria but also the prevalence of nitrate reduction (Figures 2, S1).

Under conditions where all other electron acceptors are sufficiently depleted, CO_2 may be consumed through the formation of methane in the water column or in surface sediments and

subsequently oxidized by microaerobic methanotrophs at redox transitions. Aerobic methanotrophy, being an energetically favored process (Megonigal et al., 2004), takes precedence over anaerobic oxidation on methane when sulfate and, potentially nitrate, are able to act as alternative electron acceptors. Aerobic methanotrophs synthesize 3-methylhopanoids in addition to regular hopanoids, thus, the former one has been extensively applied as a biomarker for methanotrophy. In this study, low values of 3-methylhopane index (3-MHI) (≤ 0.01), indicative of insignificant aerobic methanotrophy in the Athel deep sub-basin of the SOSB and implying an impoverished methane cycle (Table 2, Figure S1). These results are in contrast to previous work of Grosjean et al. (2009) and Stolper et al. (2017), where C_{31} 3-methylhopane was identified as a significant peak. Based on a re-evaluation of previously published data and a comparison with standards, we attribute this to the superior separation capability of the DB-5MS GC column and the specificity of the QQQ detection that combine to minimize co-elution of the 3β-methylhopane with βα-homohopane isomers and methylgammacerane. Such a phenomenon is commonly observed in other marine environments, especially when sulfate is preferred as the electron accepter. This is in agreement with previous work suggesting that SOSB was rich in sulfate (Grotzinger and Al-Rawahi, 2014). Therefore, we conclude that sulfate reduction was prevalent as a redox process in the SOSB.

The existence of sulfidic waters during deposition of SOSB sediments is supported by trace element data from Schroder and Grotzinger (2007) and Wille et al. (2008), through sulfur isotopic analyses of sulfur species by Fike and Grotzinger (2008 and 2010), and the biomarker studies of Grosjean et al. (2009) and Stolper et al. (2017). The hydrocarbon biomarker patterns evident in our analysis are entirely consistent with this, further suggesting sulfate reduction was pervasive in the Athel deep basin. For example, 28,30-dinorhopane (DNH) has been attributed to chemoautotrophic bacteria, possibly H_2S oxidizers in the chemocline (Schoell et al., 1992). Further, 25,28,30-trisnorhopane (TNH) has been proposed as a demethylation product of DNH due to the relatedness of their molecular structures. Although 25-norhopanes, in general, are often prominent in biodegraded oils (Peters et al., 2005; Schoell et al., 1992), this and prior studies have afforded no evidence for this process from the deep basinal facies of the SOSB (Grosjean et al., 2009). The ratio of (TNH+DNH)/C_{30}H ranged between 0.21 and 1.10, comparable to values reported in Stolper et al. (2017) and Grosjean et al. (2009). It displays a general pattern of increase from the U Shale to the lower Silicilyte Member and remained stable in the upper Silicilyte Member and

Thuleilat Shale (Figure 2). Although this index is highly dependent on maturity (Moldowan et al., 1984; Peters et al., 2005), other low-maturity samples deposited under anoxic/euxinic conditions display comparable values to those found in this study (Peters et al., 1994), further supporting sulfidic conditions in the water column during deposition of the SOSB deep basin (Figure 2).

In addition, a high C_{35} homohopane index (HHI; $C_{35}/C_{31\text{-}35}$) is commonly attributed to preservation of C_{35} bacteriohopanepolyols (BHP) by sulfurization as opposed to conditions where free oxygen in the water column or surface sediments can lead to oxidation of BHP to C_{31} or C_{32} homologs (Peters et al., 1995; Peters et al., 2005). Gammacerane, with its typical precursor molecule tetrahymanol being synthesized by bacterivorous ciliates, is an indicator of water column stratification (Damste et al., 1995). The homohopane index (HHI; %) and the gammacerane index ranged from 7% to 15%, and from 0.07 to 0.26, respectively (Figure 2), with an overall increasing trend upwards through the sediment column. Large variations, with no clear overall trend, were observed within the upper Silicilyte Member and Thuleilat Shale, possibly due to the limitations of sample numbers and the use of cuttings rather than core. The U Shale displayed significant differences to the Silicilyte Member ($p < 0.001$) and Thuleilat Shale ($p < 0.05$) for both parameters. Additionally, the lower and upper Silicilyte samples were remarkably different in gammacerane index ($p < 0.04$). High values of HHI, high ratios of C_{35}/C_{34} (> 1), and moderate values of gammacerane index in this study are comparable to many anoxic systems and are much higher than observed in oxidizing environments (Peters and Moldowan, 1991; Peters et al., 1994; Peters et al., 2005) (Figures 2, S1).

3.4. Euxinic photic zone or not?

The detection of a diverse assemblage of aromatic carotenoids (Appendix), biomarkers typically attributed to anoxygenic phototrophic sulfur bacteria, signals the possible presence of photic zone euxinia (Figure 5). Carotenoids with one or both end-groups aromatized are commonly proposed to be largely derived from the GSB and PSB (Brocks et al., 2005; Damsté and Koopmans, 1997; French et al., 2015; Liaaen-Jensen, 1978; van Gemerden and Mas, 1995). Okenane (IV), as the diagenetic product of okenone (III) with a single aromatic χ-ring, is a biomarker for purple sulfur bacteria (PSB) of the family Chromatiaceae that proliferate as plankton and in benthic microbial mats where the chemocline is < 24m and, in many cases, < 12m (Blankenship et al., 2006; Brocks and Schaeffer, 2008; French et al., 2015; Liaaen-Jensen and Andrewes, 1972). Similarly, chlorobactene (V), a pigment with a

single aromatic ϕ-ring characteristic of the 'green strains' of the green sulfur bacteria (GSB) family Chlorobiaceae, is the only known precursor of chlorobactane (VI), of which the detection is indicative of euxinia as shallow as 15m in the water column (Kuypers et al., 2002). Isorenieratane (XIV), with two ϕ-rings, is the diagenetic products of isorenieratene (XIII) characteristic of 'brown strains' of the GSB and is the most common carotenoid encountered in Phanerozoic marine settings (French et al., 2015). Isorenieratene-producing 'brown strains' GSB are typically observed under low light conditions and are found as deep as 100m in euxinic water columns (Overmann et al., 1992). When the chemocline is shallow, either the 'green strains' of GSB are more favored or their carotenoids are tuned differently (Bryant et al., 2012; Maresca et al., 2008b). The diaromatic carotenoid renierapurpurin (XIX), originally isolated from marine sponges and the presumed precursor of renierapurpurane (XX), possesses dual χ-rings and is the diaromatic counterpart of okenone, suggestive of an origin from PSB although direct evidence of its occurrence in cultured PSB, to our knowledge, has not been reported. Rather, the occurrence of their hydrogenated derivatives along with renieratane (XVI) and okenane (IV) in sediments has led several researchers to attribute all three compounds to sources within the Chromatiaceae (Behrens et al., 2000; Brocks et al., 2005; Brocks and Schaeffer, 2008). As with chlorobactene, the carotenoid precursor (IX) of β-isorenieratane (X) with one β-ring and one ϕ-ring is associated with communities adapted to higher light intensities than those producing isorenieratene, and therefore likely accommodate intermediate water depth (15 – 100 m) (Frigaard and Bryant, 2004; Overmann et al., 1992; Repeta, 1993).

Persistent signals of β-isorenieratane are commonly accompanied by β-paleorenieratane (VIII) (Pers. Commun. with GeoMark Research Inc.) in Neoproterozoic and Paleozoic strata, leading us to attribute them to 'brown strains' of the GSB, partially based on their structural similarities to isorenieratane and paleorenieratane, respectively (Hartgers et al., 1993). Similarly, β-renierapurpurane (XII), with its potential precursor being β-renierapurpurin (XI), have been tentatively assigned with PSB (Behrens et al., 2000; Brocks & Schaeffer, 2008). These observations, however, require further verification and are beyond the scope of the present study.

The determination of absolute carotenoid concentrations is challenging. However, because β-carotene (I) is a universal carotenoid present in the vast majority of algae and cyanobacteria,

its fossilized saturated counterpart β-carotane (II) can be used for normalization of aromatic carotenoids. Okenane, chlorobactane, β-isorenieratane, and β-paleorenieratane are present at low levels in relative to β-carotane throughout the succession (Figures 5, 6), suggestive of episodic or transient sulfide intrusion into the shallow photic zone in the Athel deep basin, especially during deposition of the U Shale and the lower Silicilyte. Comparatively, samples from A4 carbonate stringer displayed the only case where okenane is in relatively higher abundance than chlorobactane (Figure 5). So far, okenone has only been reported in modern lake settings (Brocks and Schaeffer, 2008; Meyer et al., 2011) and, as okenane, in a few ancient restricted basins (Bhattacharya et al., 2017; Brocks et al., 2005; French et al., 2015) but not in open ocean settings. Therefore, we posit that the detection and stratigraphic persistence of low levels of okenane, chlorobactane, β-isorenieratane and β-paleorenieratane in this study is consistent with restricted water circulation and transient or episodic euxinia in the shallow photic zone during deposition of the SOSB sedimentary sequence. Transient euxinia is possibly disturbed by periodic seawater incursion into the restricted basin and is further corroborated by the detection of biomarkers indicative of sponges, which survive in oxic and suboxic conditions (Mills et al., 2014).

Signals of isorenieratane were near the detection limit in our samples from the Athel deep basin. This is in contrast to the carbonate platform, exemplified by A4 carbonate stringer from Birba-3 well, where isorenieratane was detected in minute traces. Since the carbonate platform was presumably deposited under relatively shallower water than the Silicilyte, it seems possible that the isorenieratane found in the platform could be benthic microbial mats derived when the sediment-water interface was sulfidic under reducing conditions. Comparatively, barely detectable isorenieratane in the deep basin deposits might be attributed to sharply diminishing light intensity to the deep depth where ‘brown strains’ of GSB are competitive (Connock et al., 2018), possibly due to light absorption by shallow water sulfur bacteria and shading by a dense oxygenic phototrophic community, as supported by the detection of steranes and hopanes. Another possibility is that the deep water was ferruginous that sulfide in the deep water has been scavenged by excessive iron (Fike & Grotzinger, 2010), suppressing the productivity of low-light-adapted GSB. Alternatively, minimal isorenieratene may not be interpreted as an absence of ‘brown strains’ of GSB inhabiting deeper water depths. Indeed, in studies on modern lake systems where there is rDNA evidence for the presence of GSB in the photic zone, isorenieratene (XIII) is either not detected (Meyer et al., 2011) or detected at trace levels (Fulton et al., 2018) when the

chemocline is shallow (e.g., 6-20m) (Glaeser and Overmann, 2003; Meyer et al., 2011). Well-studied examples of modern environments include Fayetteville Green Lake near Syracuse in New York, which is a small, meromictic kettle lake with steep sides and limited wind fetch such that seasonal overturn is precluded (Meyer et al., 2011).

Renierapurpurane (XX) and renieratane (XVI) show comparable abundances to β-isorenieratane (X) and are much higher than isorenieratane (Figures 5, S4). Both compounds have been proposed as being derived from PSB (Behrens et al., 2000; Brocks et al., 2005; Brocks & Schaeffer, 2008). In this study, ratios of (renieratane+renierapurpurane) / β-carotane, with ranges between 0.04 and 0.33, have a poor correlation with (okenane+chlorobactene) / β-carotane ($R^2 < 0.2$) and a weak correlation with (β-paleorenieratane+ β-isorenieratane) / β-carotane ($R^2 = 0.46$), suggestive of different sources. Rather, the latter two proxies mimic each other and show strong correlation ($R^2 = 0.76$; Figure 7). Consequently, our results suggest multiple sources for the above-mentioned compounds and question the sulfur bacterial origin of renierapurpurane and renieratane. Interestingly, predominant renierapurpurane and renieratane have been detected in the Green River Fm. and Barney Creek Fm. (Brocks et al., 2005; French et al., 2020). French et al. (2020) attributed this pattern, and the abundant co-occurring 3β-methylhopanes, to these rocks having been deposited in lacustrine settings, an explanation that does not apply to the restricted marine environment of the sediments studied here. An alternative origin for renierapurpurane is from cyanobacteria. Our alternative hypothesis is based on the distribution of lipids reported from the euryhaline, unicellular taxon *Synechococcus* sp. strain PCC 7002 and relates species, which synthesize renierapurpurin (XIX) as an intermediate in the biosynthesis of the cyanobacterial carotenoid χ,χ-caroten-18,18'-dioic acid (XXV), otherwise known as synechoxanthin, via the intermediates XXI, XXII and XXIV (Graham and Bryant, 2008; Graham et al., 2008). Further research has confirmed production of renieratene and traces of isorenieratene from these strains (Cui et al., 2020). Studies of the presence of synechoxanthin in *Synechococcus* sp. PCC7002 implicate CruH as the protein that is minimally responsible for the hydroxylation/oxidation of the C-18 and C-18' methyl groups of renierapurpurin (Graham and Bryant, 2008; Montero et al., 2011). Taking this logic further, we propose that compounds XXI, XXII and XXIV, through diagenetic hydrogenation and loss of one or both of these substituents from the structures and thermally-driven decarboxylation reactions, could produce XXIII and XXVI, that is, C_{39} and C_{38} diagenetic products (Appendix).

C_{39} and C_{38} carotenoid diagenesis products are tentatively identified in this study. One of them, as a major compound, was observed to elute between β-renierapurpurane and isorenieratane and has a molecular ion of 532 Da with major fragment ions of 134, 133, and 120 Da. These features identity this compound as a C_{39} diaryl isoprenoid with trimethyl substitution in one ring and a dimethyl substitution in the other (Figure S4). In earlier work, Schwark and Püttmann (1990) reported a C_{39} diaryl isoprenoid at a similar relative retention position and containing one less methylene carbon in the isoprenoid chain. However, subsequent investigation deemed this unlikely and, instead, identified a set of C_{40} tetra-aromatic carotenoids with the same molecular weight of 532 Da (Koopmans et al., 1996). None of these compounds were reported to have 120 Da as a major fragment ion (>50% of 134) making the compound reported here distinct. A second major compound identified in the Athel-1 and Birba-3 sediments is a C_{38} diaromatic aryl isoprenoid based on its relative retention time and an MRM transition employing precursor and product ions of 518 and 120 Da (Figure S4). Knowing that decarboxylation is a facile, thermally-driven process during catagenesis, we hypothesized that synechoxanthin (XXV) could be its potential biogenic precursor. This hypothesis was reinforced by a report from Koopmans et al. (1997) who identified the same C_{38} dimethyl/dimethyl diaromatic carotenoid in the Green River Shale and another by Zhang et al. (2011) who identified C_{39} and C_{38} aryl isoprenoids but speculated that they resulted from the loss of a methyl group from one or both aromatic rings.

We sought additional support for our hypothesis by examining the relative abundance ratios of different carotenoid and the respective diagenesis products. In this, we observed a strong correlation between the ratios of the C_{39} carotenoid /β-carotane and (renieratane + renierapurpurane) / β-carotane which suggests that they may be biologically or diagenetically related (Figure 7). Therefore, the detection of a distinctive biomarker assemblage in this study comprising a predominance of renierapurpurane and renieratane together with putative C_{39} and C_{38} diagenetic products, and the strong correlation mentioned above, point to cyanobacteria as an alternate and most likely source for these carotenoids (Graham and Bryant, 2008; Graham et al., 2008).

3.5 Implications of the SOSB carotenoid data

It has been suggested that the presence of phototrophic sulfur bacteria in the water column, or in microbial mats, and the types of carotenoids produced by them, are highly linked. For example, the monoaromatic carotenoids are regarded as molecular indicators of high-light-

adapted PSB and GSB dependent upon shallow chemoclines or representing inputs from microbial mats. Diaromatic carotenoids are typically attributed to low-light-adapted GSB dwelling in chemoclines at up to 100 m depth (Overmann, 2008). In this study, no correlation was found between (chlorobactene + okenane) / β-carotane and (renieratane + reneirapurpurane) / β-carotane ($p > 0.3$), suggesting multiple independent sources and/or multiple controlling factors. Notably, while renierapurpurin does not appear to have been identified in cultured PSB, it has been reported in a cultured cyanobacterium (Graham and Bryant, 2008; Graham et al., 2008), which is further supported by this study. Further, the biosynthesis of aromatic carotenoids has been observed in other cyanobacteria and, accordingly, does not require sulfidic water columns nor PZE (Maresca et al., 2008a).

We also observed that (β-paleorenieratane + β-isorenieratane) / β-carotane displayed a weak but significant correlation with (renieratane + reneirapurpurane) / β-carotane ($p<0.001$), and a stronger correlation with (chlorobactane+okenane) / β-carotane ($p<0.001$; Figure 7). Considering no correlation between (chlorobactene + okenane) / β-carotane and (renieratane + renierapurpurane) / β-carotane, it suggests that organisms producing β-paleorenieratene and β-isorenieratene (IX) may also have more complex sources than previously recognized. Although β-isorenieratene has been proven to be synthesized by GSB, β-renierapurpurin (XI) and, potentially, other bicyclic monoaromatic carotenoids are also intermediates along the biosynthesis pathway leading to aromatic carotenoids in cyanobacteria and streptomyces as well (Graham & Bryant, 2008).

In this study, the C_{39} carotenoid/β-carotane ratio across many samples presented a strong correlation with (renieratane+renierapurpurane) / β-carotane, suggesting a source relationship. Additionally, the C_{39} compound (XXIII) was in higher abundances compared to renieratane (XVI) and renierapurpurane (XX), suggesting that the depositional environment favored the production of its carotenoid precursor. Furthermore, the C_{38} compound (XXVI) is either comparable or sometimes more abundant compared to its C_{39} counterpart, also speaking to their close linkage. Dimethyl aryl isoprenoids have been reported in high concentrations in hypersaline environments (Damsté et al., 1988; Koopmans et al., 1997; Zhang et al., 2011). All of these observations point to the possibility that high concentrations of C_{38} and C_{39} carotenoids are associated with hypersaline conditions as opposed to PZE. However, their presence in SOSB does not negate the possibility that the SOSB was sulfate rich at the Ediacaran-Cambrian Boundary, but instead provides another potential explanation for the

presence of C_{40} diaromatic carotenoids (e.g., renierapurpurane) and their unusual distribution pattern in this case study. Additionally, based on our observations, C_{38} and C_{39} carotenoids found in the deep basinal package of the Athel Fm. are much higher than in the Buah Fm. and the carbonate platform units (Figure 5), making them potentially valuable proxies for oil-source correlation.

Conclusions

This study demonstrates that the composition of microbial communities varied significantly during the deposition of the U Shale, Silicilyte and Thuleilat Shale members of the Athel Formation in the Athel deep basin across the Ediacaran-Cambrian Boundary. Specifically, sterane/hopane ratios and other indices indicate shifts in plankton communities and water chemistry (e.g., stratification, nutrients), possibly driven by tectonism and the subsequent episodic connection of the restricted basin to the open ocean. The three units investigated in this study witnessed a progressive increase in water column stratification following fresh seawater intrusion in the U Shale.

Absent evidence for a significant methane cycle and a weak denitrification-induced nitrogen fixation, our data suggest that sulfate reduction was the preferred terminal respiratory process. The presence, albeit low concentrations, of monoaromatic (e.g., chlorobactene, okenane) carotenoids synthesized by anoxygenic photosynthetic purple and green sulfur bacteria supports episodic or transient euxinic conditions in the shallow photic zone of the Athel sub-basin or, possibly, input from microbial mats. Barely detectable isorenieratane in the Athel deep basin implies minimal deep-water adapting “brown strain” green sulfur bacteria, possibly due to 1) shading of planktonic microbial communities; 2) a ferruginous deep ocean; or minimal synthesis of isorenieratene by GSB under some conditions. Comparatively, the unusual predominance of renieratane and renierapurpurane over isorenieratane, together with abundances of C_{39} and C_{38} carotenoids in the Athel deep basin and their strong statistical correlation, identifies cyanobacteria is the most probable contributor to the diaromatic carotenoid inventory. Overall, we propose that the aromatic carotenoids present in Ediacaran strata may have sources other than phototrophic sulfur bacteria. Further detailed investigations of aromatic carotenoids in other taxa such as the cyanobacteria will improve the robustness of paleoenvironmental reconstructions.

Acknowledgements

679 We gratefully acknowledge financial support from the NASA Astrobiology Institute
680 (NNA13AA90A) and the Simons Foundation Collaboration on the Origins of Life
681 (290361FY18). This work benefitted from discussions with Professor Donald Bryant of The
682 Pennsylvania State University, concerning the origins of synechoxanthin and discussions with
683 Don Rocher and John Zumberge of GeoMark Research Inc. on aromatic carotenoids. We
684 thank the Ministry of Oil and Gas of the Sultanate of Oman for permission to access samples.
685 Petroleum Development Oman contributed subsurface sample access.
686

687

688 Table 1: Major biomarkers applied in this study and their source indications.

689

Parameters	Interpretation	References
Acyclic isoprenoids		
pristane/phytane	water column redox	Didyk et al. (1978)
Hopanes		
Ts/(Ts+Tm)	thermal maturity index/ lithology	Farrimond et al. (1998)
C_{31}H S/(S+R)	thermal maturity index	Seifert and Moldowan (1980)
(TNH+DNH)/C_{30}H	photic zone sulfur cycle	Schoell et al. (1992)
gammacerane/C_{30}H	stratification	Schoell et al. (1994)
2-MHI	cyanobacteria or N2-fixing bacteria	Summons et al. (1999); Kuypers et al. (2004)
3-MHI	intensity of methanotroph	Summons et al. (1994)
C_{35} HHI	water column redox condition	Peters and Moldowan (1991)
Sterane		
C_{29} dia/(dia+reg)	thermal maturity index	van Kaam-Peters et al. (1998)
C_{29}/($C_{27+28+29}$)	green vs red algae	Schwark and Empt (2006)
C_{30}-npc	marine algae; sponges	Moldowan et al. (1990); Love et al. (2009)
C_{30}-ipc	sponges	Love et al. (2009)
C_{30}-26-methylstigmastane	sponges	Zumberge et al. (2018)
Carotenoids		
chlorobactane	green sulfur bacteria	Grice et al. (1998)
okenane	purple sulfur bacteria	Schaeffer et al. (1997)
isorenieratane	green sulfur bacteria	Summons and Powell (1987); Maresca et al. (2008b)
renieratane	green/purple sulfur bacteria or cyanobacteria	Schaefle et al. (1977); Hartgers et al. (1993) This Study
renierapurpurane	purple sulfur bacteria or	Schaefle et al. (1977); (Brocks et al., 2005)

	cyanobacteria	This Study
β-paleorenieratane	green sulfur bacteria	Hartgers et al. (1993); This Study
β-isorenieratane	green sulfur bacteria or cyanobacteria	Grice et al. (1998); Schaeffer et al. (1997); this study
β-renierapurpurane	purple sulfur bacteria or cyanobacteria	Behrens et al. (2000); Schaeffer et al. (1997) This Study
C_{39} carotenoid	cyanobacteria	This Study
C_{38} carotenoid	cyanobacteria	This Study

690

691

692

693

694

Table 2. The average and standard deviation of parameters in each formation, where the Silicilyte is divided into the upper and lower Silicilyte formations.

	Thuleilat Shale	Upper Silicilyte	Lower Silicilyte	"U" Shale	Buah	Shuram	Carbonate Platform
$\delta^{13}C$ (‰)	-38.9±1.5	-37.8±0.4	-37.0±0.7	-36.2±1.7	-37.9±0.0	-36.5±1.5	-35.0[a]
$\delta^{15}N$ (‰)	3.0±1.2	3.1±0.3	3.3±0.3	2.4±0.5	2.9±1.0	2.5±1.2	5.8[a]
pristane/phytane	0.55±0.16	0.27±0.12	0.20±0.07	0.31±0.07	0.67±0.04	0.60±0.09	0.43±0.20
Ts/(Ts+Tm)	0.24±0.02	0.23±0.02	0.25±0.02	0.24±0.04	0.16±0.02	0.54±0.25	0.18±0.00
(TNH+DNH)/C_{30}H[a]	0.76±0.16	0.77±0.03	0.70±0.35	0.39±0.07	0.21±0.08	0.08±0.08	0.62±0.03
C_{30}H βα/(αβ+βα)	0.04±0.00	0.03±0.01	0.03±0.00	0.03±0.00	0.03±0.00	0.03±0.00	0.03±0.00
C_{31}H S/(S+R)	0.52±0.01	0.55±0.00	0.56±0.01	0.55±0.01	0.53±0.00	0.56±0.02	0.57±0.00
gammacerane/C_{30}H	0.21±0.05	0.19±0.02	0.13±0.05	0.09±0.01	0.30±0.09	0.16±0.08	0.20±0.01
C_{35}/(C_{31-35})H (%)	11.6±1.0	12.6±2.4	10.3±2.3	7.5±0.5	10.7±4.0	7.9±2.2	9.9±0.3
2-MHI (%)[b]	11.3±2.2	11.7±1.0	9.5±0.9	7.9±0.5	12.4±0.8	9.1±1.9	5.6±0.1
3-MHI (%)[c]	1.00±0.19	0.66±0.04	0.51±0.08	0.70±0.16	0.83±0.08	0.63±0.14	0.81±0.03
27-nor C_{26}/(C_{26-30})S (%)[d]	15.8±3.9	9.4±2.4	6.9±1.5	11.3±3.3	9.7±3.2	8.4±1.9	7.8±0.0
C_{27}/(C_{26-30})S (%)[d]	20.0±1.3	18.2±1.3	15.7±1.3	19.6±1.5	22.3±2.4	17.7±3.0	20.6±1.3
C_{28}/(C_{26-30})S (%)[d]	12.7±0.1	12.7±0.8	12.3±0.4	13.5±1.0	11.0±0.6	11.3±1.4	11.3±0.4
C_{29}/(C_{26-30})S (%)[d]	49.2±4.2	57.4±2.7	63.1±3.3	53.2±5.9	54.7±6.5	60.5±6.0	57.9±0.9
C_{30}/(C_{26-30})S (%)[d]	2.3±0.1	2.2±0.2	2.1±0.2	2.4±0.5	2.3±0.3	2.2±0.3	2.4±0.1
C_{30}S ipc/npc[e]	0.94±0.02	0.83±0.03	0.96±0.10	0.67±0.15	0.55±0.05	0.84±0.19	0.82±0.09
3β-me C_{29}/C_{29} S[f]	0.25±0.01	0.22±0.02	0.31±0.09	0.29±0.04	0.25±0.10	0.35±0.12	0.25±0.00
C_{29}S dia/(dia+reg)[g]	0.06±0.02	0.03±0.01	0.02±0.00	0.04±0.01	0.03±0.01	0.11±0.07	0.04±0.00
C_{29}S aaa S/(S+R)[h]	0.51±0.01	0.49±0.01	0.50±0.00	0.49±0.02	0.50±0.00	0.51±0.01	0.51±0.00
sterane/hopane[i]	0.49±0.06	0.64±0.01	0.61±0.04	0.76±0.09	0.72±0.21	0.59±0.10	0.66±0.11
(chl+oke)/β-carotane[j]	0.14±0.01	0.18±0.03	0.20±0.07	0.31±0.12	0.18±0.04	0.27±0.09	0.11±0.01
(β-pal+β-iso) /β-carotane[k]	0.70±0.15	0.47±0.15	0.41±0.08	0.58±0.14	0.29±0.06	0.49±0.15	0.28±0.00
(ren+rnp) /β-carotane[l]	0.23±0.09	0.19±0.03	0.11±0.05	0.14±0.06	0.06±0.02	0.09±0.07	0.05±0.00
C_{39} carotenoid /β-carotane	0.68±0.27	0.61±0.08	0.39±0.12	0.33±0.08	0.09±0.02	0.20±0.16	0.10±0.00

[a] only one sample was measured for OC and N isotopes.

[b] 2-methylhopane index (2-MHI) is calculated as: C_{30-34} 2-methylhopanes/(C_{30-34} 2-methylhopanes+ C_{30-34} hopanes).

[c] 3-methylhopane index (3-MHI) is calculated as: $C_{30\text{-}32}$ 3-methylhopanes/($C_{30\text{-}32}$ 3-methylhopanes+ $C_{30\text{-}32}$ hopanes).

[d] $C_{26\text{-}30}$ steranes include diasteranes (βα and αβ) and regular steranes (5α, 14α, 17α and 5α, 14β, 17β) of 27-nor C_{26}, C_{27}, C_{28}, C_{29} and C_{30}-npc and C_{30}-ipc.

[e] calculated based on 20R 5α, 14α, 17α C_{30}-npc and C_{30}-ipc steranes.

[f] calculated based only on regular 3β-me C_{29} and C_{29} steranes.

[g] C_{29}S dia/(dia+reg) represents C_{29} diasterane/(C_{29} diasterane+C_{29} regular sterane)

[h] calculated based on 20S and 20R 5α, 14α, 17α C_{29} steranes.

i calculated based on $C_{27\text{-}29}$ diasteranes and regular steranes, $C_{27\text{-}30}$ hopanes, and $C_{31\text{-}35}$ homohopanes.

[j] chl: chlorobactene; oke: okenane

[k] β-pal: β-paleorenieratane; β-iso: β-isorenieratane

[l] ren: renieratane; rnp: renierapurpurane

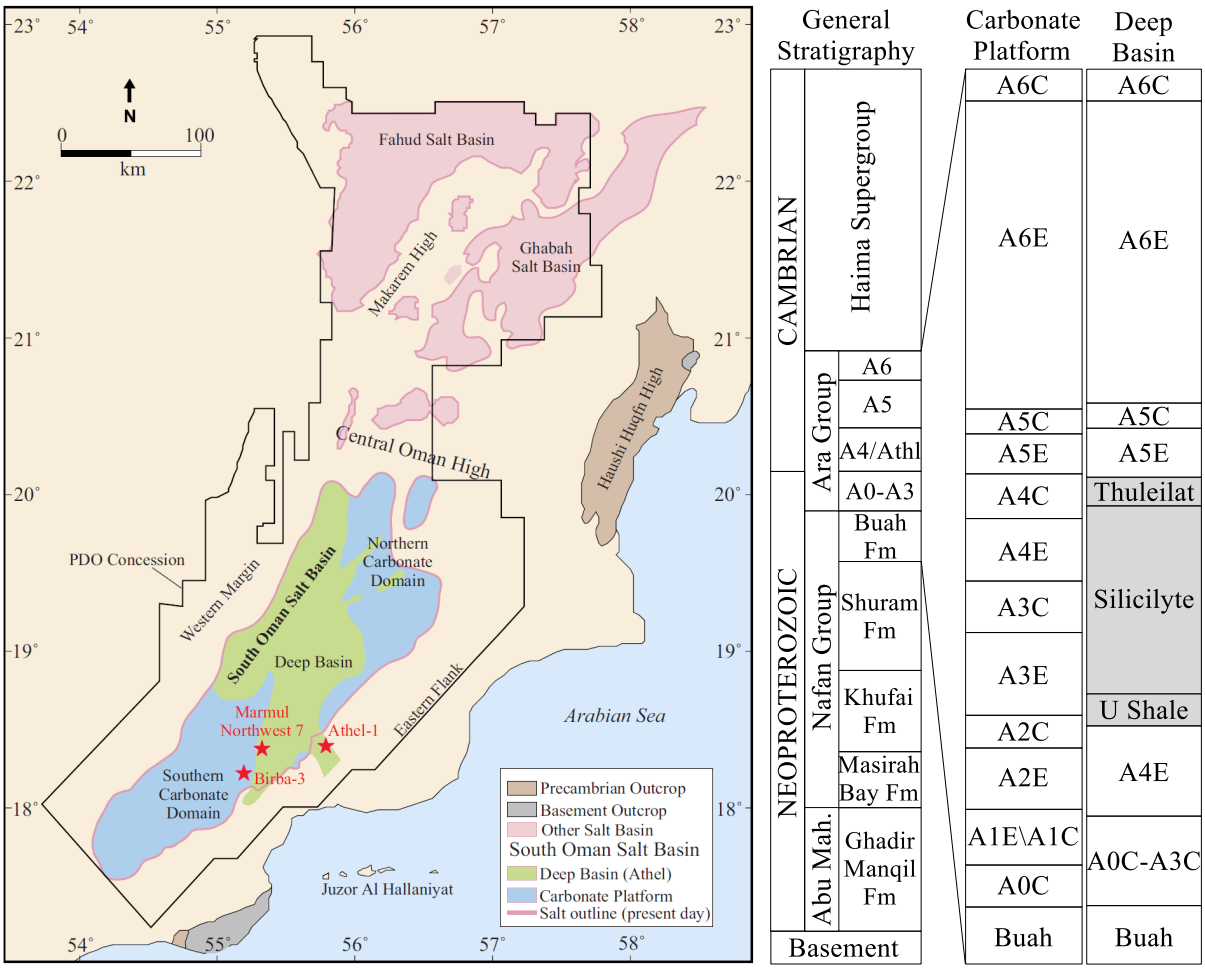

Figure 1. Map and stratigraphy of the South Oman Salt Basin, where the A4 carbonates from the platform are time equivalent to the U Shale + Athel Silicilyte Formation + Thuleilat Shale in the deep sub-basin. The shaded area represents the time period investigated in this study. The figures are modified from Al-Siyabi (2005) and Grotzinger and Al-Rawahi (2014).

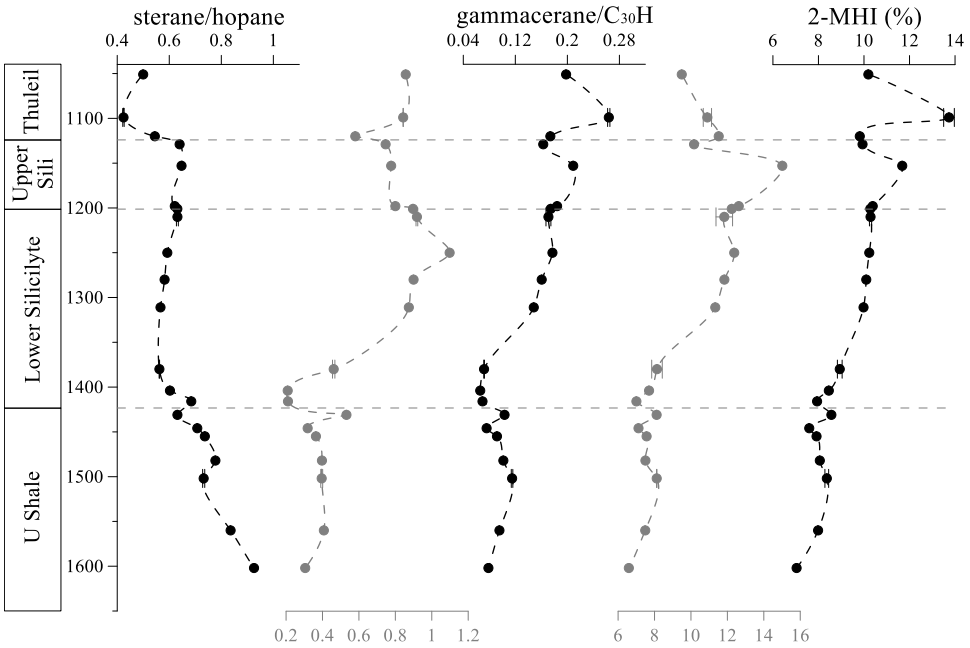

Figure 2. Downcore profiles of sterane/hopane ratios, selected hopanes, and gammacerane. The numbers represent downcore depths in meters, while the grey dashed lines represent formation boundaries. TNH: 25,28,30-trinorhopane; DNH: 28,30-dinorhopane; HHI: homohopane index, defined as the percentage of $C_{35}/(C_{31\text{-}35})$ homohopanes; 2-MHI: 2-methylhopane index.

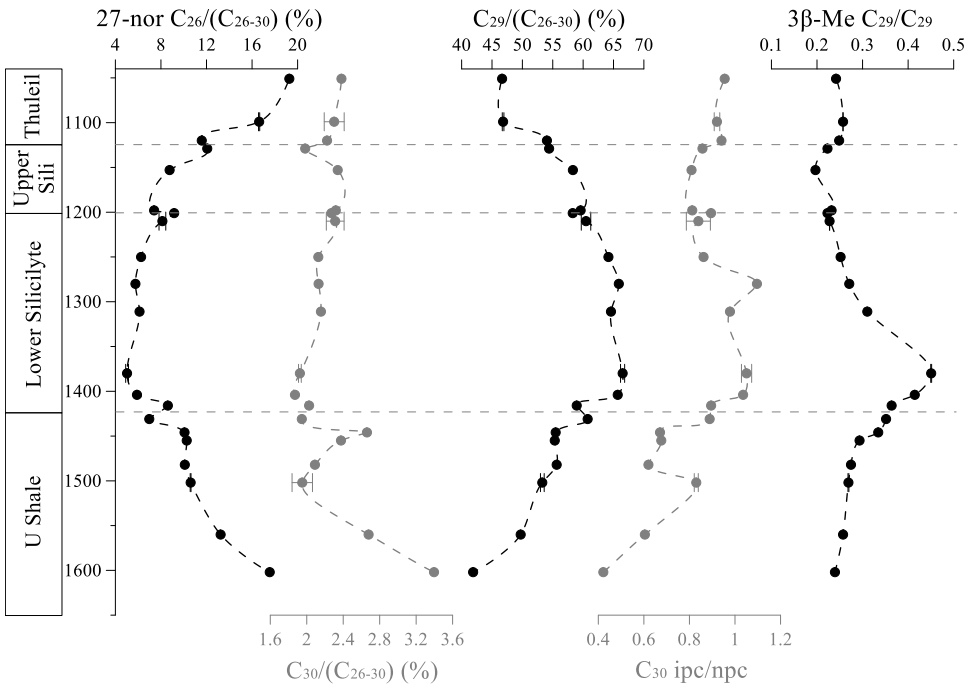

Figure 3. Downcore profiles of selected sterane indices. C_{30} ipc: C_{30} 24-isopropyl cholestane; C_{30} npc: C_{30} 24-n-propyl cholestane, 3β-Me C_{29}: 3β-methyl-24-ethyl cholestane.

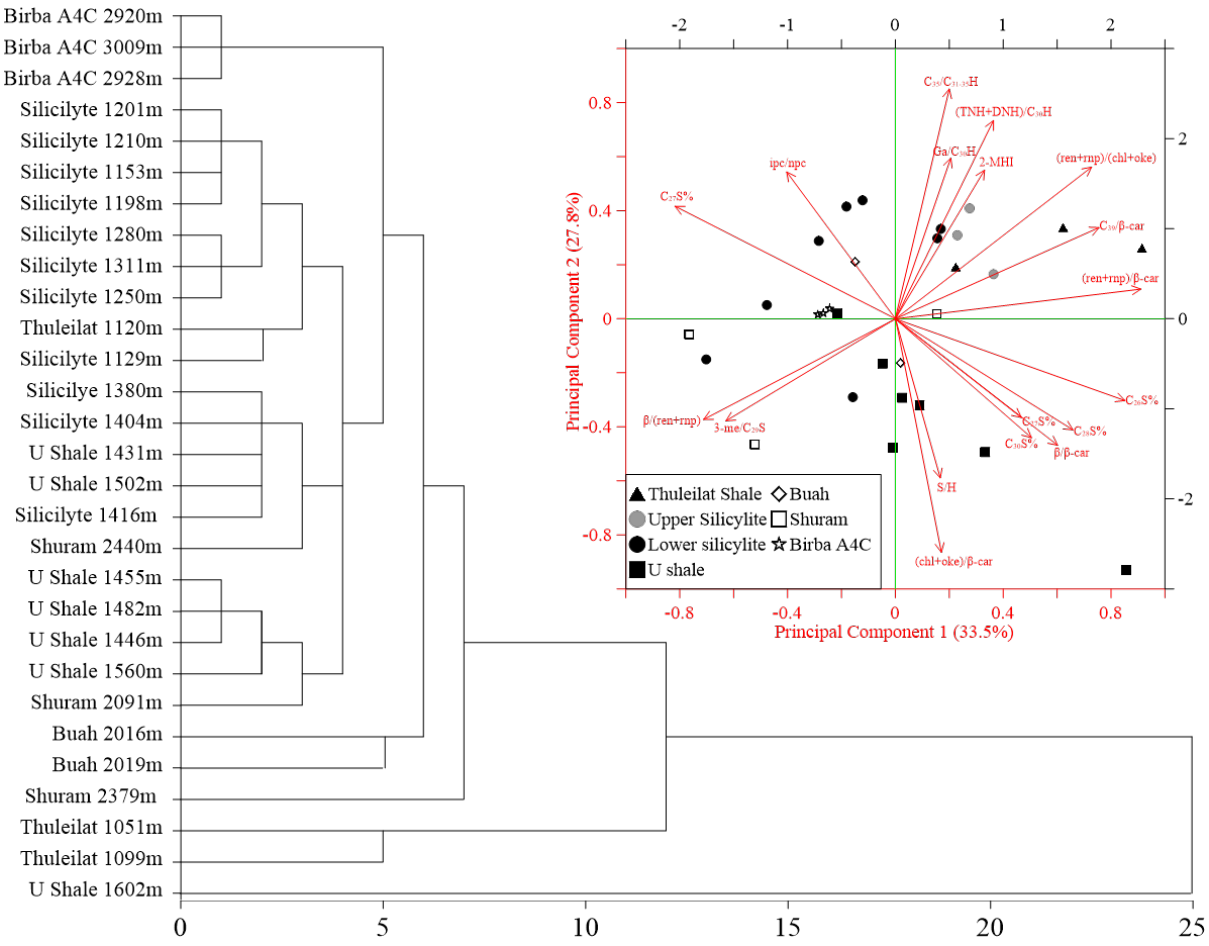

Figure 4. Comprehensive data analysis, including cluster analysis and principal component analysis (PCA). Cluster analysis is performed based on sterane, hopane, and carotenoid indices. The specific molecular proxies included in the cluster analysis are $C_{28}/(C_{26\text{-}30})$ steranes, $C_{29}/(C_{26\text{-}30})$ steranes, $C_{30}/(C_{26\text{-}30})$ steranes, C_{30} sterane ipc/npc, (TNH+DNH)/C_{30} hopane, 2-MHI, sterane/hopane ratio, (chl+oke)/β-carotane, (β-pal+β-iso)/β-carotane, (ren+rnp)/β-carotane, C_{39} carotenoid/β-carotane. Principal component analysis, seen in the upper right corner, is performed with all parameters indicated in the plot. Parameters are represented in red arrows, while each sample is displayed using variable symbol. TNH: trisnorhopane; DNH: dinorhopane; chl: chlorobactene; oke: okenane; β-pal: β-paleorenieratane; β-iso: β-isorenieratane; ren: renieratane; rnp: reneirapurpurane.

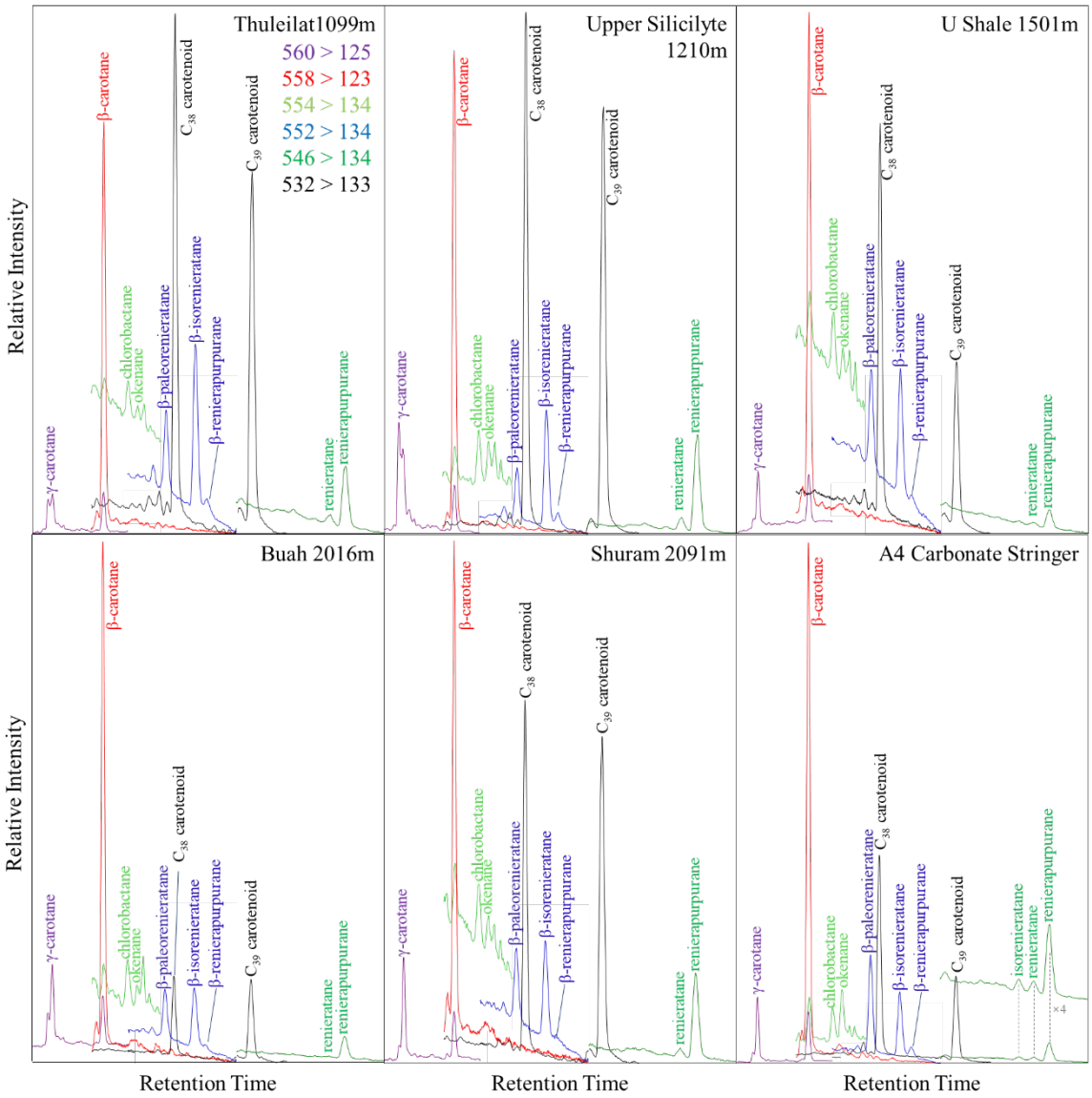

Figure 5. Composite MRM reaction chromatograms of selected saturated and aromatic carotenoid biomarkers from each representative unit studied in this study. The response of each compound is shown in intensity normalized to the most intense peak. Chromatograms are coloured according to their specific reactions in the MRM mode. The upper three samples from Thuleilat Shale, Silicilyte Formation, and U Shale are shown in comparison with examples from Buah Formation, Shuram Formation and A4 Carbonate Stringer.

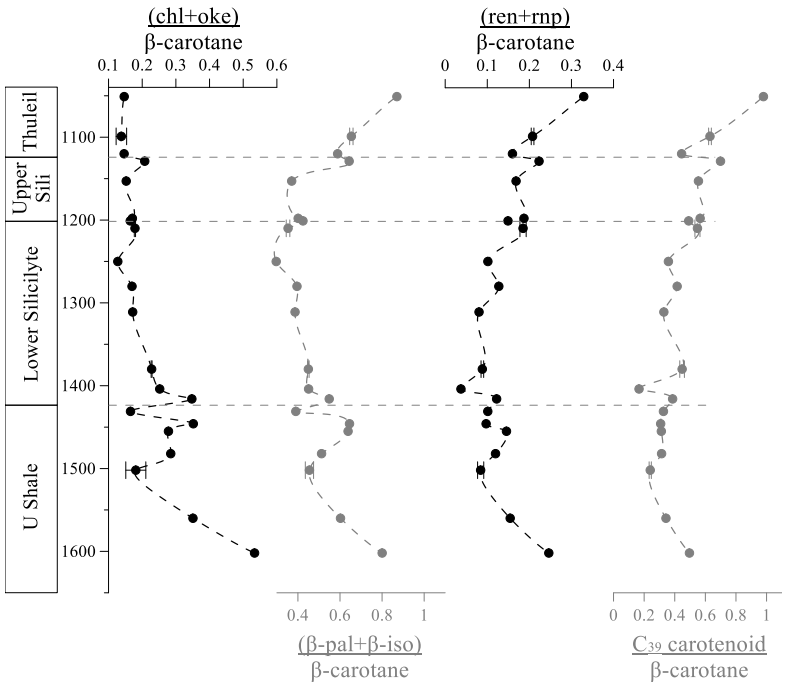

763

764 Figure 6. Downcore profiles of selected carotenoid indices. chl: chlorobactene; oke: okenane;
765 β-pal: β-paleorenieratane; β-iso: β-isorenieratane; ren: renieratane; rnp: renierapurpurane; C_{39}
766 carotenoid: new compound reported in this study with precursor and product ions of 532Da
767 and 134Da, respectively.

768

769

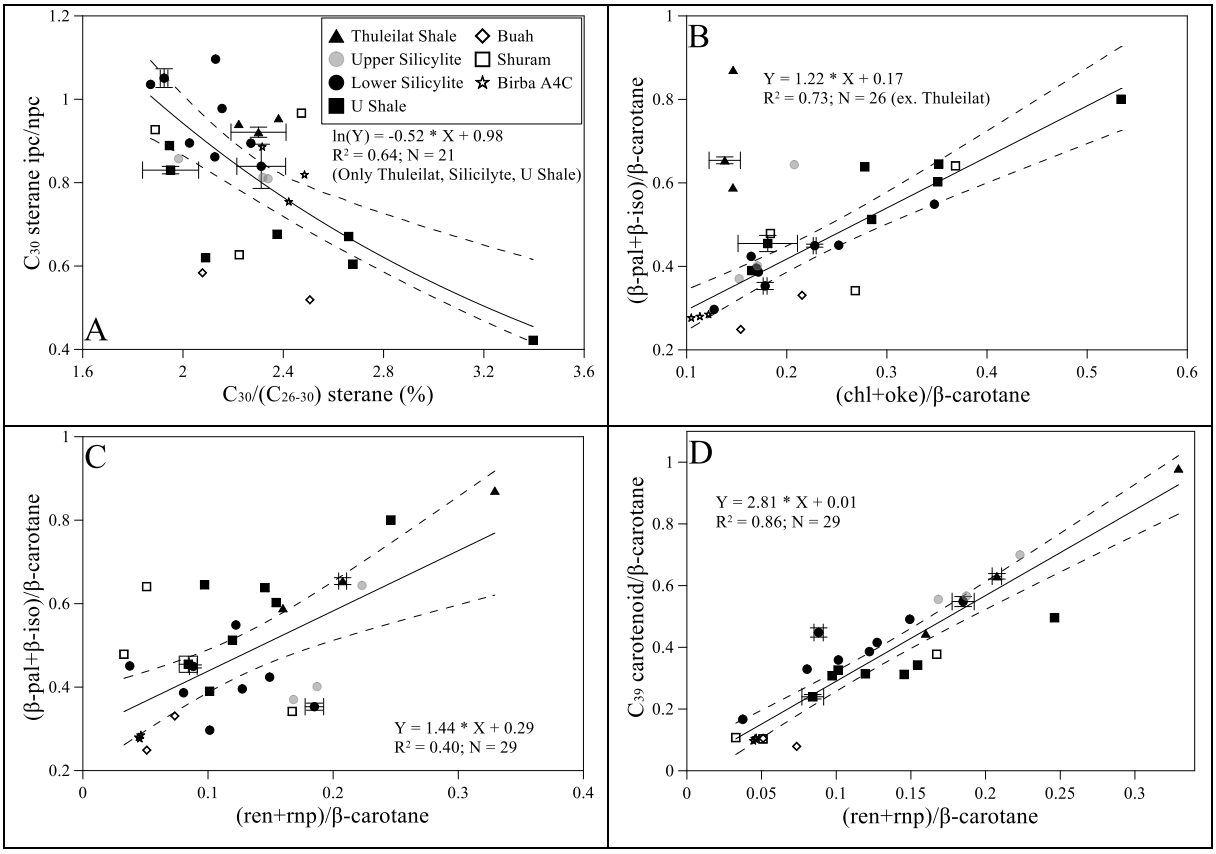

Figure 7. The cross plots of selected sterane and carotenoid-based indices. The regressions are chosen based on the best fits. The abbreviations are explained in preceding figures and tables.

APPENDIX

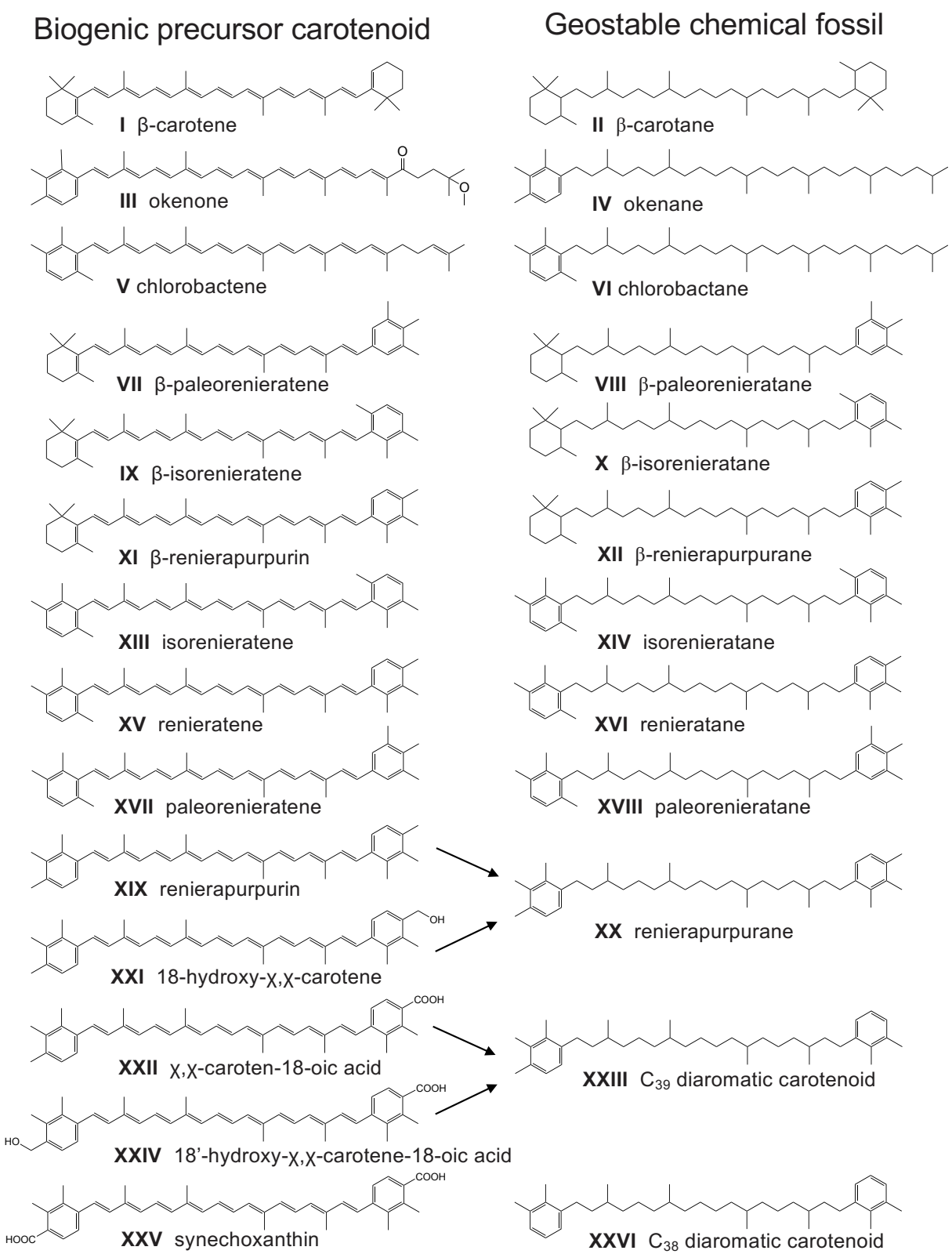

Appendix. Structures of carotenoids pertinent to this study. Arrows designate putative diagenetic transformations of synechoxanthin and its biosynthetic precursors.

References:

Aitken, J. (1966) Middle Cambrian to Middle Ordovician cyclic sedimentation, southern Rocky Mountains of Alberta. Bulletin of Canadian Petroleum Geology 14, 405-441.

Al Rajaibi, I.M., Hollis, C., Macquaker, J.H. and Pufahl, P. (2015) Origin and variability of a terminal Proterozoic primary silica precipitate, Athel Silicilyte, South Oman Salt Basin, Sultanate of Oman. Sedimentology 62, 793-825.

Al-Siyabi, H.A. (2005) Exploration history of the Ara intrasalt carbonate stringers in the South Oman Salt Basin. GeoArabia 10, 39-72.

Allen, P.A. (2007) The Huqf Supergroup of Oman: Basin development and context for Neoproterozoic glaciation. Earth-Science Reviews 84, 139-185.

Amend, J.P. and Shock, E.L. (2001) Energetics of overall metabolic reactions of thermophilic and hyperthermophilic Archaea and Bacteria. FEMS microbiology reviews 25, 175-243.

Amthor, J., Faulkner, T., Frewin, N., Alixant, J., Matter, A. and Ramseyer, K. (1998) The Athel play in Oman: controls on reservoir quality. GeoArabia 3, 61-62.

Amthor, J.E., Grotzinger, J.P., Schröder, S. and Schreiber, B.C. (2002) Tectonically-Driven Evaporite–Carbonate Transitions in a Precambrian/Cambrian Saline Giant: Ara Salt Basin of South Oman, American Association of Petroleum Geologists Annual Convention, March 10–13th, Houston, Abstract Volume, pp. A6-7.

Amthor, J.E., Ramseyer, K., Matter, A., Pettke, T. and Fallick, A.E. (2015) Diagenesis of a light, tight-oil chert reservoir at the Ediacaran/Cambrian boundary, Sultanate of Oman. GeoArabia 20, 147-178.

Behrens, A., Schaeffer, P., Bernasconi, S. and Albrecht, P. (2000) Mono-and bicyclic squalene derivatives as potential proxies for anaerobic photosynthesis in lacustrine sulfur-rich sediments. Geochimica et Cosmochimica Acta 64, 3327-3336.

Bhattacharya, S., Dutta, S. and Summons, R.E. (2017) A distinctive biomarker assemblage in an Infracambrian oil and source rock from western India: Molecular signatures of eukaryotic sterols and prokaryotic carotenoids. Precambrian Research 290, 101-112.

Blankenship, R.E., Madigan, M.T. and Bauer, C.E. (2006) Anoxygenic photosynthetic bacteria. Springer Science & Business Media.

Bowring, S.A., Grotzinger, J.P., Condon, D.J., Ramezani, J., Newall, M.J. and Allen, P.A. (2007) Geochronologic constraints on the chronostratigraphic framework of the Neoproterozoic Huqf Supergroup, Sultanate of Oman. American Journal of Science 307, 1097-1145.

Brocks, J.J., Jarrett, A.J., Sirantoine, E., Hallmann, C., Hoshino, Y. and Liyanage, T. (2017) The rise of algae in Cryogenian oceans and the emergence of animals. Nature 548, 578.

Brocks, J.J., Love, G.D., Summons, R.E., Knoll, A.H., Logan, G.A. and Bowden, S.A. (2005) Biomarker evidence for green and purple sulphur bacteria in a stratified Palaeoproterozoic sea. Nature 437, 866.

Brocks, J.J. and Schaeffer, P. (2008) Okenane, a biomarker for purple sulfur bacteria (Chromatiaceae), and other new carotenoid derivatives from the 1640 Ma Barney Creek Formation. Geochimica et Cosmochimica Acta 72, 1396-1414.

Bryant, D.A., Liu, Z., Li, T., Zhao, F., Costas, A.M.G., Klatt, C.G., Ward, D.M., Frigaard, N.-U. and Overmann, J. (2012) Comparative and functional genomics of anoxygenic green bacteria from the taxa Chlorobi, Chloroflexi, and Acidobacteria, Functional genomics and evolution of photosynthetic systems. Springer, pp. 47-102.

Canfield, D.E., Farquhar, J. and Zerkle, A.L. (2010) High isotope fractionations during sulfate reduction in a low-sulfate euxinic ocean analog. Geology 38, 415-418.

828 Connock, G.T., Nguyen, T.X. and Philp, R.P. (2018) The development and extent of photic-
829 zone euxinia concomitant with Woodford Shale deposition. AAPG Bulletin 102, 959-986.
830 Cui, X., Liu, X.-L., Shen, G., Ma, J., Husain, F., Rocher, D., Zumberge, J.E., Bryant, D.A.
831 and Summons, R.E. (2020) Niche expansion for phototrophic sulfur bacteria at the
832 Proterozoic-Phanerozoic transition. Proceedings of the National Academy of Sciences
833 Accepted pending revisions.
834 Damsté, J.S. and Koopmans, M.P. (1997) The fate of carotenoids in sediments: an overview.
835 Pure and applied chemistry 69, 2067-2074.
836 Damsté, J.S.S., Kock-van Dalen, A. and de Leeuw, J.W. (1988) Identification of long-chain
837 isoprenoid alkylbenzenes in sediments and crude oils. Geochimica et Cosmochimica Acta 52,
838 2671-2677.
839 Didyk, B., Simoneit, B., Brassell, S.t. and Eglinton, G. (1978) Organic geochemical indicators
840 of palaeoenvironmental conditions of sedimentation. Nature 272, 216.
841 Erwin, D.H. (2015) Early metazoan life: divergence, environment and ecology. Philosophical
842 Transactions of the Royal Society B: Biological Sciences 370, 20150036.
843 Farrimond, P., Taylor, A. and TelnÆs, N. (1998) Biomarker maturity parameters: the role of
844 generation and thermal degradation. Organic Geochemistry 29, 1181-1197.
845 Fike, D. and Grotzinger, J. (2008) A paired sulfate–pyrite δ34S approach to understanding the
846 evolution of the Ediacaran–Cambrian sulfur cycle. Geochimica et Cosmochimica Acta 72,
847 2636-2648.
848 Fike, D. and Grotzinger, J. (2010) A δ34SSO4 approach to reconstructing biogenic pyrite
849 burial in carbonate-evaporite basins: An example from the Ara Group, Sultanate of Oman.
850 Geology 38, 371-374.
851 Fike, D., Grotzinger, J., Pratt, L. and Summons, R. (2006) Oxidation of the Ediacaran ocean.
852 nature 444, 744.
853 Forbes, G., Jansen, H. and Schreurs, J. (2010) Lexicon of Oman subsurface stratigraphy.
854 GeoArabia 15, 210-215.
855 French, K., Rocher, D., Zumberge, J. and Summons, R. (2015) Assessing the distribution of
856 sedimentary C 40 carotenoids through time. Geobiology 13, 139-151.
857 French, K.L., Tosca, N.J., Cao, C. and Summons, R.E. (2012) Diagenetic and detrital origin
858 of moretane anomalies through the Permian–Triassic boundary. Geochimica et Cosmochimica
859 Acta 84, 104-125.
860 Frigaard, N.-U. and Bryant, D.A. (2004) Seeing green bacteria in a new light: genomics-
861 enabled studies of the photosynthetic apparatus in green sulfur bacteria and filamentous
862 anoxygenic phototrophic bacteria. Archives of microbiology 182, 265-276.
863 Fulton, J.M., Arthur, M.A., Thomas, B. and Freeman, K.H. (2018) Pigment carbon and
864 nitrogen isotopic signatures in euxinic basins. Geobiology 16, 429-445.
865 Glaeser, J. and Overmann, J. (2003) Characterization and in situ carbon metabolism of
866 phototrophic consortia. Applied and environmental microbiology 69, 3739-3750.
867 Gold, D.A., Grabenstatter, J., de Mendoza, A., Riesgo, A., Ruiz-Trillo, I. and Summons, R.E.
868 (2016) Sterol and genomic analyses validate the sponge biomarker hypothesis. Proceedings of
869 the National Academy of Sciences, 201512614.
870 Grabenstatter, J., Méhay, S., McIntyre-Wressnig, A., Giner, J.-L., Edgcomb, V.P., Beaudoin,
871 D.J., Bernhard, J.M. and Summons, R.E. (2013) Identification of 24-n-propylidenecholesterol
872 in a member of the Foraminifera. Organic geochemistry 63, 145-151.
873 Graham, J.E. and Bryant, D.A. (2008) The biosynthetic pathway for synechoxanthin, an
874 aromatic carotenoid synthesized by the euryhaline, unicellular cyanobacterium
875 Synechococcus sp. strain PCC 7002. Journal of Bacteriology 190, 7966-7974.

Graham, J.E., Lecomte, J.T.J. and Bryant, D.A. (2008) Synechoxanthin, an aromatic C40 xanthophyll that is a major carotenoid in the cyanobacterium Synechococcus sp. PCC 7002. Journal of Natural Products 71, 1647-1650.
Grantham, P., Lijmbach, G., Posthuma, J., Clarke, M.H. and Willink, R. (1988a) Origin of crude oils in Oman. Journal of Petroleum Geology 11, 61-80.
Grantham, P.J., Lijmbach, J., Posthuma, J., Hughes Clarke, M.W. and Willink, R.J. (1988b) Origin of Crude Oils in Oman. Journal of Petroleum Geology 11, 61-88.
Grice, K., Schouten, S., Peters, K.E. and Damsté, J.S.S. (1998) Molecular isotopic characterisation of hydrocarbon biomarkers in Palaeocene–Eocene evaporitic, lacustrine source rocks from the Jianghan Basin, China. Organic Geochemistry 29, 1745-1764.
Grosjean, E., Love, G., Stalvies, C., Fike, D. and Summons, R. (2009) Origin of petroleum in the Neoproterozoic–Cambrian South Oman salt basin. Organic Geochemistry 40, 87-110.
Grotzinger, J. and Al-Rawahi, Z. (2014) Depositional facies and platform architecture of microbialite-dominated carbonate reservoirs, Ediacaran–Cambrian Ara Group, Sultante of Om. AAPG Bulletin 98, 1453-1494.
Grotzinger, J., Al-Siyabi, A., Al-Hashimi, R. and Cozzi, A. (2002) New model for tectonic evolution of Neoproterozoic-Cambrian Huqf Supergroup basins, Oman. GeoArabia 7, 241.
Gurnis, M. (1988) Large-scale mantle convection and the aggregation and dispersal of supercontinents. Nature 332, 695.
Gurnis, M. (1992) Rapid continental subsidence following the initiation and evolution of subduction. Science 255, 1556-1558.
Hallmann, C., Nettersheim, B.J., Brocks, J.J., Schwelm, A., Hope, J.M., Not, F., Lomas, M., Schmidt, C., Schiebel, R., Nowack, E.C.M., De Deckker, P., Pawlowski, J., Bowser, S.S., Bobrovskiy, I., Zonneveld, K., Kucera, M. and Stuhr, M. (2019) Reply to: Sources of C30 steroid biomarkers in Neoproterozoic–Cambrian rocks and oils. Nature Ecology & Evolution.
Hartgers, W.A., Damsté, J.S.S., Koopmans, M.P. and de Leeuw, J.W. (1993) Sedimentary evidence for a diaromatic carotenoid with an unprecedented aromatic substitution pattern. Journal of the Chemical Society, Chemical Communications, 1715-1716.
Harvey, H.R. and Mcmanus, G.B. (1991) Marine ciliates as a widespread source of tetrahymanol and hopan-3β-ol in sediments. Geochimica et Cosmochimica Acta 55, 3387-3390.
Koopmans, M.P., De Leeuw, J.W. and Damsté, J.S.S. (1997) Novel cyclised and aromatised diagenetic products of β-carotene in the Green River Shale. Organic Geochemistry 26, 451-466.
Koopmans, M.P., Köster, J., Van Kaam-Peters, H.M., Kenig, F., Schouten, S., Hartgers, W.A., de Leeuw, J.W. and Damsté, J.S.S. (1996) Diagenetic and catagenetic products of isorenieratene: molecular indicators for photic zone anoxia. Geochimica et Cosmochimica Acta 60, 4467-4496.
Kuypers, M.M., Pancost, R.D., Nijenhuis, I.A. and Sinninghe Damsté, J.S. (2002) Enhanced productivity led to increased organic carbon burial in the euxinic North Atlantic basin during the late Cenomanian oceanic anoxic event. Paleoceanography 17, 3-1-3-13.
Kuypers, M.M., van Breugel, Y., Schouten, S., Erba, E. and Damsté, J.S.S. (2004) N2-fixing cyanobacteria supplied nutrient N for Cretaceous oceanic anoxic events. Geology 32, 853-856.
Leavitt, W.D., Halevy, I., Bradley, A.S. and Johnston, D.T. (2013) Influence of sulfate reduction rates on the Phanerozoic sulfur isotope record. Proceedings of the National Academy of Sciences 110, 11244-11249.
Liaaen-Jensen, S. (1978) Chemistry of carotenoid pigments. Photosynthetic bacteria, 233-247.
Liaaen-Jensen, S. and Andrewes, A. (1972) Microbial carotenoids. Annual Reviews in Microbiology 26, 225-248.

Love, G.D., Grosjean, E., Stalvies, C., Fike, D.A., Grotzinger, J.P., Bradley, A.S., Kelly, A.E., Bhatia, M., Meredith, W. and Snape, C.E. (2009) Fossil steroids record the appearance of Demospongiae during the Cryogenian period. Nature 457, 718.
Love, G.D., Zumberge, J.A., Cárdenas, P., Sperling, E.A., Rohrssen, M., Grosjean, E., Grotzinger, J.P. and Summons, R.E. (2019) Sources of C30 steroid biomarkers in Neoproterozoic–Cambrian rocks and oils. Nature Ecology & Evolution.
Maresca, J., Graham, J. and Bryant, D. (2008a) The biochemical basis for structural diversity in the carotenoids of chlorophototrophic bacteria. Photosynthesis Research 97, 121-140.
Maresca, J.A., Romberger, S.P. and Bryant, D.A. (2008b) Isorenieratene biosynthesis in green sulfur bacteria requires the cooperative actions of two carotenoid cyclases. Journal of bacteriology 190, 6384-6391.
Megonigal, J.P., Hines, M.E. and Visscher, P.T. (2004) Anaerobic metabolism: linkages to trace gases and aerobic processes. Biogeochemistry.
Meyer, K., Macalady, J., Fulton, J., Kump, L., Schaperdoth, I. and Freeman, K. (2011) Carotenoid biomarkers as an imperfect reflection of the anoxygenic phototrophic community in meromictic Fayetteville Green Lake. Geobiology 9, 321-329.
Mills, B., Lenton, T.M. and Watson, A.J. (2014) Proterozoic oxygen rise linked to shifting balance between seafloor and terrestrial weathering. Proceedings of the National Academy of Sciences.
Moldowan, J.M., Fago, F.J., Lee, C.Y., Jacobson, S.R., Watt, D.S., Slougui, N.-E., Jeganathan, A. and Young, D.C. (1990) Sedimentary 12-n-propylcholestanes, molecular fossils diagnostic of marine algae. Science 247, 309-312.
Moldowan, J.M., Seifert, W.K., Arnold, E. and Clardy, J. (1984) Structure proof and significance of stereoisomeric 28, 30-bisnorhopanes in petroleum and petroleum source rocks. Geochimica et Cosmochimica Acta 48, 1651-1661.
Moldowan, J.M., Seifert, W.K. and Gallegos, E.J. (1985) Relationship between petroleum composition and depositional environment of petroleum source rocks. AAPG bulletin 69, 1255-1268.
Moldowan, J.M., Sundararaman, P. and Schoell, M. (1986) Sensitivity of biomarker properties to depositional environment and/or source input in the Lower Toarcian of SW-Germany. Organic Geochemistry 10, 915-926.
Montero, O., Porta, J.M., Porta, J., Martínez, G. and Lubián, L.M. (2011) Characterization of two Synechococcus sp. PCC7002-related cyanobacterial strains in relation to 16S rDNA, crtR gene, lipids and pigments. Phycological Research 59, 147-155.
Nettersheim, B.J., Brocks, J.J., Schwelm, A., Hope, J.M., Not, F., Lomas, M., Schmidt, C., Schiebel, R., Nowack, E.C.M. and De Deckker, P. (2019) Putative sponge biomarkers in unicellular Rhizaria question an early rise of animals. Nature ecology & evolution 3, 577-581.
Overmann, J. (2008) Ecology of phototrophic sulfur bacteria, Sulfur Metabolism in Phototrophic Organisms. Springer, pp. 375-396.
Overmann, J., Cypionka, H. and Pfennig, N. (1992) An Extremely Low-Light-Adapted Phototrophic Sulfur Bacterium from the Black Sea. Limnology and Oceanography 37, 150-155.
Pehr, K., Love, G.D., Kuznetsov, A., Podkovyrov, V., Junium, C.K., Shumlyanskyy, L., Sokur, T. and Bekker, A. (2018) Ediacara biota flourished in oligotrophic and bacterially dominated marine environments across Baltica. Nature communications 9, 1807.
Peters, K., Clark, M., Gupta, U.D., McCaffrey, M. and Lee, C. (1995) Recognition of an infracambrian source rock based on biomarkers in the Baghewala-1 oil, India. AAPG bulletin 79, 1481-1493.

974 Peters, K. and Moldowan, J. (1991) Effects of source, thermal maturity, and biodegradation
975 on the distribution and isomerization of homohopanes in petroleum. Organic Geochemistry
976 17, 47-61.
977 Peters, K.E., Kontorovich, A.E., Huizinga, B.J., Moldowan, J.M. and Lee, C.Y. (1994)
978 Multiple oil families in the West Siberian Basin. AAPG bulletin 78, 893-909.
979 Peters, K.E., Peters, K.E., Walters, C.C. and Moldowan, J. (2005) The biomarker guide.
980 Cambridge university press.
981 Repeta, D.J. (1993) A high resolution historical record of Holocene anoxygenic primary
982 production in the Black Sea. Geochimica et Cosmochimica Acta 57, 4337-4342.
983 Schaeffer, P., Adam, P., Wehrung, P. and Albrecht, P. (1997) Novel aromatic carotenoid
984 derivatives from sulfur photosynthetic bacteria in sediments. Tetrahedron Letters 38, 8413-
985 8416.
986 Schaefle, J., Ludwig, B., Albrecht, P. and Ourisson, G. (1977) Hydrocarbures aromatiques
987 d'origine geologique. II: Nouveaux Carotanoïdes Aromatiques Fossiles. Tetrahedron Letters
988 18, 3673-3676.
989 Schiefelbein, C.F., Zumberge, J., Cameron, N. and Brown, S. (1999) Petroleum systems in the
990 South Atlantic margins. Geological Society, London, Special Publications 153, 169-179.
991 Schoell, M., Hwang, R., Carlson, R. and Welton, J. (1994) Carbon isotopic composition of
992 individual biomarkers in gilsonites (Utah). Organic Geochemistry 21, 673-683.
993 Schoell, M., McCaffrey, M., Fago, F. and Moldowan, J. (1992) Carbon isotopic compositions
994 of 28, 30-bisnorhopanes and other biological markers in a Monterey crude oil. Geochimica et
995 Cosmochimica Acta 56, 1391-1399.
996 Schroder, S. and Grotzinger, J. (2007) Evidence for anoxia at the Ediacaran–Cambrian
997 boundary: the record of redox-sensitive trace elements and rare earth elements in Oman.
998 Journal of the Geological Society 164, 175-187.
999 Schröder, S., Schreiber, B.C., Amthor, J.E. and Matter, A. (2003) A depositional model for
1000 the terminal Neoproterozoic–Early Cambrian Ara Group evaporites in south Oman.
1001 Sedimentology 50, 879-898.
1002 Schwark, L. and Empt, P. (2006) Sterane biomarkers as indicators of palaeozoic algal
1003 evolution and extinction events. Palaeogeography, Palaeoclimatology, Palaeoecology 240,
1004 225-236.
1005 Schwark, L. and Püttmann, W. (1990) Aromatic hydrocarbon composition of the Permian
1006 Kupferschiefer in the Lower Rhine basin, NW Germany. Organic Geochemistry 16, 749-761.
1007 Seifert, W. and Moldowan, J.M. (1986) Use of biological markers in petroleum exploration.
1008 Methods in geochemistry and geophysics 24, 261-290.
1009 Seifert, W.K. and Moldowan, J.M. (1980) The effect of thermal stress on source-rock quality
1010 as measured by hopane stereochemistry. Physics and Chemistry of the Earth 12, 229-237.
1011 Sim, M.S., Bosak, T. and Ono, S. (2011) Large Sulfur Isotope Fractionation Does Not
1012 Require Disproportionation. Science 333, 74.
1013 Stolper, D., Love, G., Bates, S., Lyons, T., Young, E., Sessions, A. and Grotzinger, J. (2017)
1014 Paleoecology and paleoceanography of the Athel silicilyte, Ediacaran–Cambrian boundary,
1015 Sultanate of Oman. Geobiology 15, 401-426.
1016 Summons, R. and Powell, T. (1987) Identification of aryl isoprenoids in source rocks and
1017 crude oils: biological markers for the green sulphur bacteria. Geochimica et cosmochimica
1018 acta 51, 557-566.
1019 Summons, R.E., Jahnke, L.L., Hope, J.M. and Logan, G.A. (1999) 2-Methylhopanoids as
1020 biomarkers for cyanobacterial oxygenic photosynthesis. Nature 400, 554.
1021 Summons, R.E., Jahnke, L.L. and Roksandic, Z. (1994) Carbon isotopic fractionation in lipids
1022 from methanotrophic bacteria: relevance for interpretation of the geochemical record of
1023 biomarkers. Geochimica et Cosmochimica Acta 58, 2853-2863.

Terken, J.M., Frewin, N. and Indrelid, S. (2001) Petroleum systems of Oman: charge timing and risks. AAPG bulletin 85, 1817-1845.
van Gemerden, H. and Mas, J. (1995) Ecology of phototrophic sulfur bacteria, Anoxygenic photosynthetic bacteria. Springer, pp. 49-85.
van Kaam-Peters, H.M., Köster, J., van der Gaast, S.J., Dekker, M., de Leeuw, J.W. and Damsté, J.S.S. (1998) The effect of clay minerals on diasterane/sterane ratios. Geochimica et Cosmochimica Acta 62, 2923-2929.
Whiteside, J.H. and Grice, K. (2016) Biomarker records associated with mass extinction events. Annual Review of Earth and Planetary Sciences 44, 581-612.
Wille, M., Nägler, T.F., Lehmann, B., Schröder, S. and Kramers, J.D. (2008) Hydrogen sulphide release to surface waters at the Precambrian/Cambrian boundary. Nature 453, 767.
Zhang, C., Zhang, Y. and Cai, C. (2011) Aromatic isoprenoids from the 25–65 Ma saline lacustrine formations in the western Qaidam Basin, NW China. Organic geochemistry 42, 851-855.
Zumberge, J.A., Love, G.D., Cárdenas, P., Sperling, E.A., Gunasekera, S., Rohrssen, M., Grosjean, E., Grotzinger, J.P. and Summons, R.E. (2018) Demosponge steroid biomarker 26-methylstigmastane provides evidence for Neoproterozoic animals. Nature ecology & evolution 2, 1709.

Supplementary Information

Table S1. Major compounds analyzed in this study and the precursor and products *m/z* values used to detect them through MRM transitions.

Target Compound	Precursor	Product	Target Compound	Precursor	Product
C_{26} steranes	358	217	C_{27} trinor(neo)hopanes	370	191
C_{27} steranes	372	217	C_{27} trinorhopane	370	177
C_{28} steranes	386	217	C_{28} dinorhopane	384	191
C_{29} steranes	400	217	C_{29} norhopane	398	191
C_{30} steranes	414	217	C_{30} hopanes, gammacerane	412	191
C_{30} methyl steranes	414	231	C_{31} homohopanes	426	191
β-carotane	558	123	C_{32} homohopanes	440	191
γ-carotane	560	125	C_{33} homohopanes	454	191
chlorobactane	554	134	C_{34} homohopanes	468	191
okenane	554	134	C_{35} homohopanes	482	191
isorenieratane	546	134	C_{31} methyl hopanes	426	205
renieratane	546	134	C_{32} methyl hopanes	440	205
renierapurpurane	546	134	C_{33} methyl hopanes	454	205
β-series carotenoids	552	134	C_{34} methyl hopanes	468	205
C_{39} carotenoids	532	134	C_{35} methyl hopanes	482	205
C_{38} carotenoids	518	134			

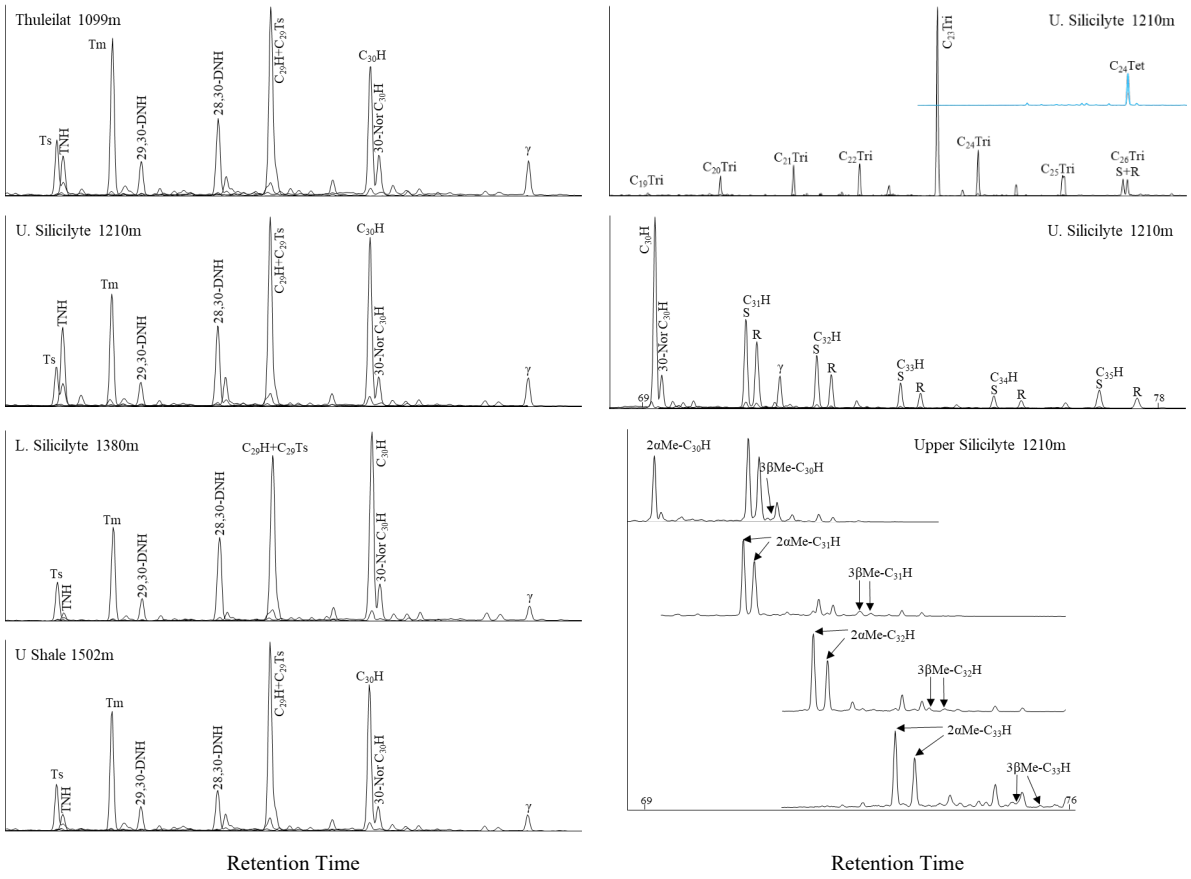

Figure S1. Representative GCMS data for hopanes, gammacerane, and tricyclic terpanes depicted using the summation of the responses of the precursor-product transitions generated using MRM data acquisition. $C_{27\text{-}30}$ hopanes and gammacerane (γ) are shown in the left panel, while tricyclic terpanes, C_{24} tetracyclic terpane, homohopanes, and methylhopanes in the right panel. Each group of biomarkers has different range of retention time. Note the numbers in homohopane and methylhopane figures are indicative of retention times.

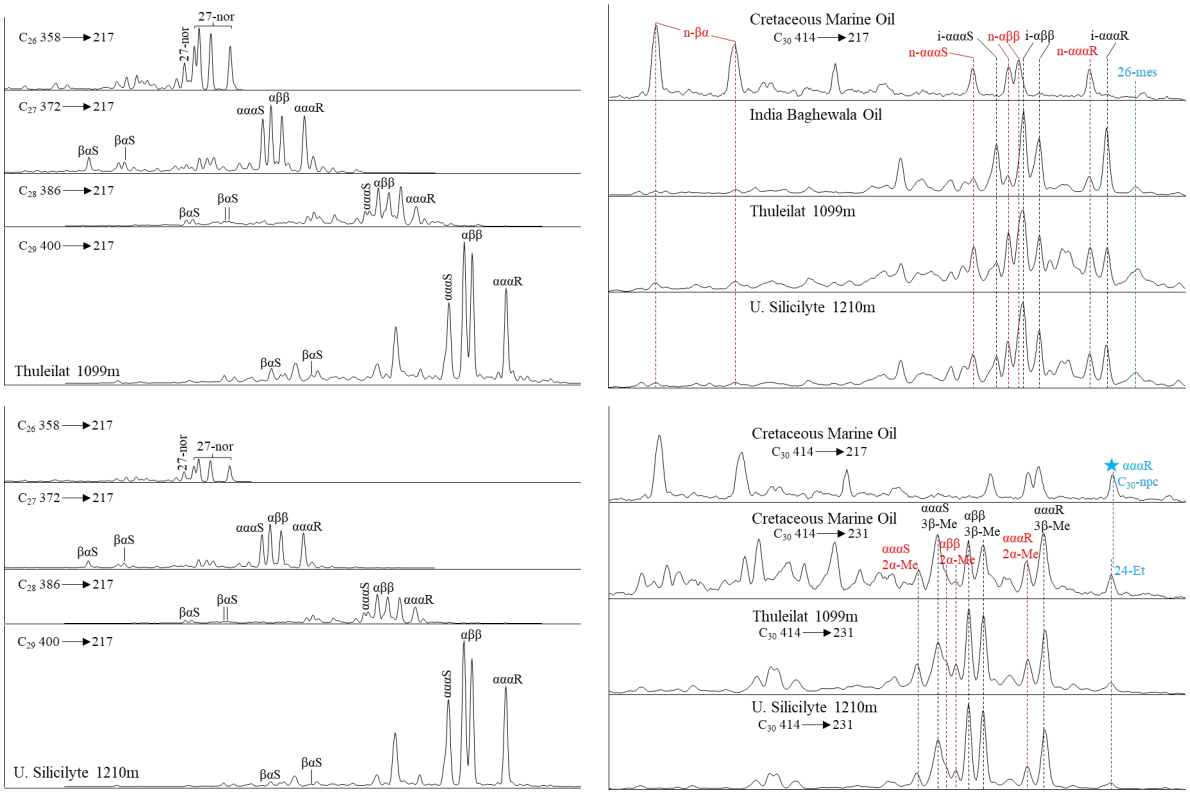

Figure S2. Representative GCMS data for steranes depicted using the summation of the responses of the precursor-product transitions generated using MRM data acquisition. C_{26}-C_{29} steranes are shown in the left panel and C_{30} methyl- and desmethylsteranes in the right panel. Each group of biomarkers has different range of retention time.

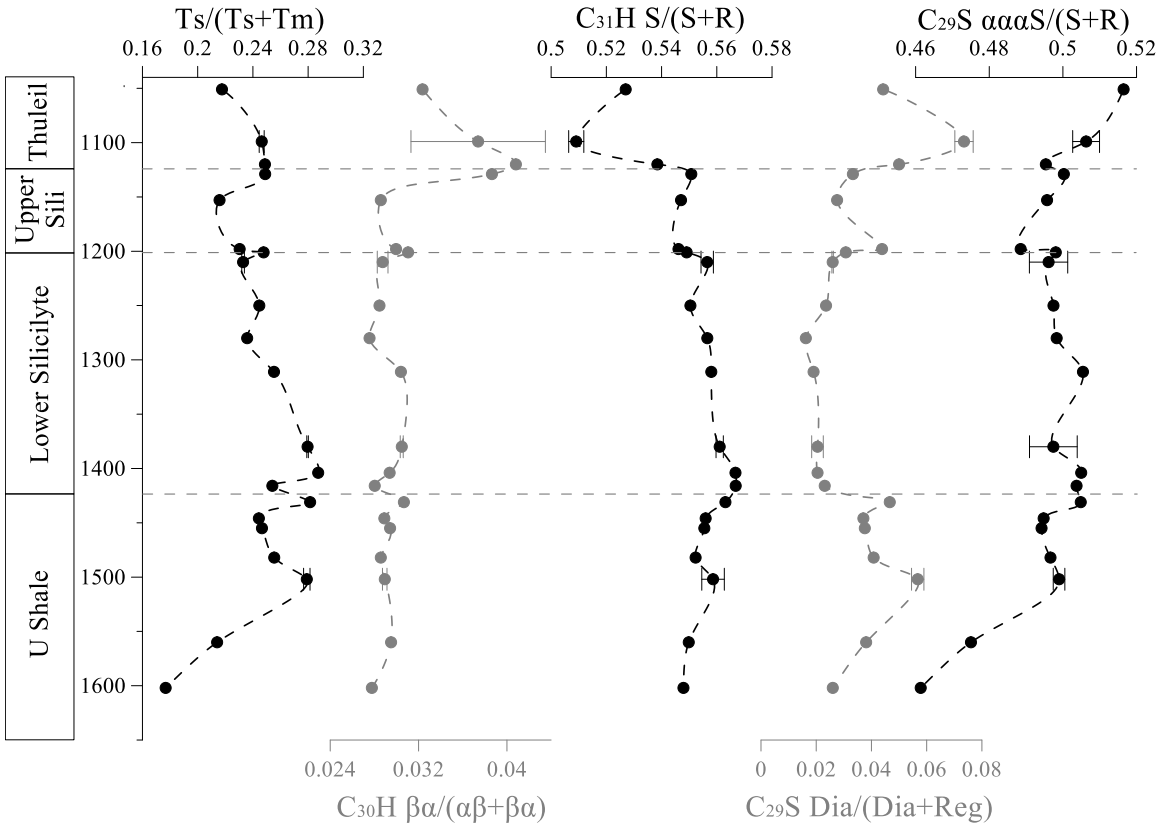

Figure S3. The downcore profiles of maturity sensitive parameters, including Ts/(Ts+Tm), C_{30}H βα/(αβ+βα), C_{31}H S/(S+R), $C_{27\text{-}29}$S dia/(dia+reg), and C_{29}s ααS/(S+R), where Ts is 18α-22,29,30-trisnorneohopane, Tm is 17β-22,29,30-trisnorhopane, C_{30}H is C_{30} hopane, C_{31}H is C_{31} homohopane, C_{29}S is C_{29} sterane.

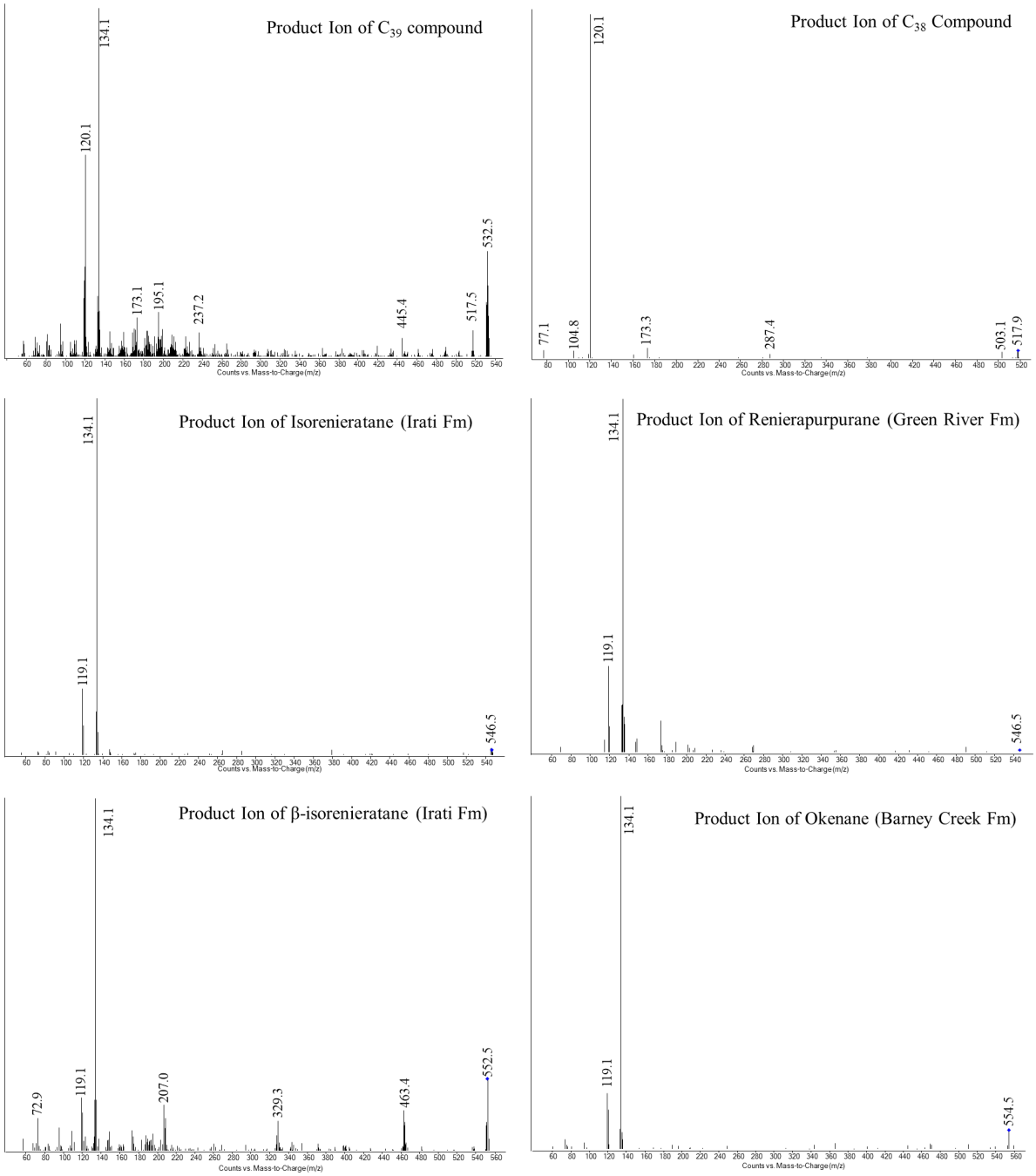

Figure S4. Product ion spectra of the molecular ions of the C_{39} and C_{38} diaromatic carotenoids proposed to be the diagenetic products of synechoxanthin. For comparison, are the product ion spectra of isorenieratane, renierapurpurane, β-isorenieratane, and okenane from a variety of reference sediments where they are abundant.